A myeloid program associated with COVID-19 severity is decreased by therapeutic blockade of IL-6 signaling

Jason A. Hackney[#1], Haridha Shivram[#1], Jason Vander Heiden[1], Chris Overall[1], Luz Orozco[1], Xia Gao[1], Nathan West, Aditi Qamra[2], Diana Chang[1], Arindam Chakrabarti[1], David F. Choy[1], Alexis J. Combes[3], Tristan Courau[3], Gabriela K. Fragiadakis[3], Arjun Arkal Rao[3], Arja Ray[3], Jessica Tsui[3], Kenneth Hu[3], Nicholas F. Kuhn[3], Matthew F. Krummel[3], David J. Erle[3], Kirsten Kangelaris[3], Aartik Sarma[3], Zoe Lyon[3], Carolyn S. Calfee[3], Prescott G. Woodruff[3], Rajani Ghale[3], Eran Mick[3], Ashley Byrne[3], Shoshana Zha[3], Charles Langelier[3], Carolyn M. Hendrickson[3], Monique G.P. van der Wijst[4], George C. Hartoularos[3], Tianna Grant[3], Raymund Bueno[3], David S. Lee[3], John R. Greenland[3], Yang Sun[3], Richard Perez[3], Anton Ogorodnikov[3], Alyssa Ward[3], Chun Jimmie Ye[3], UCSF COMET Consortium[3], Thiru Ramalingam[1], Jacqueline M. McBride[1], Fang Cai[1], Anastasia Teterina[2], Min Bao[1], Larry Tsai[1], Ivan O. Rosas[5], Aviv Regev[1], Sharookh B. Kapadia[1], Rebecca N. Bauer[1], Carrie M. Rosenberger[1*]

1. Genentech, Inc. 1 DNA Way, South San Francisco, CA 94080, USA.
2. Hoffman-La Roche Limited. 7070 Mississauga Road. Mississauga, ON L5N 5M8 Canada
3. University of California San Francisco, San Francisco, CA, USA.
4. Department of Genetics, University of Groningen, University Medical Center Groningen, Groningen, The Netherlands.
5. Baylor College of Medicine, 7200 Cambridge St, Houston, TX 77030, USA
[#]J.A. Hackney and H. Shivram contributed equally to this work.

*Corresponding author: Carrie M Rosenberger, Rosenberger.carrie@gene.com , 1-650-467-9065

Additional UCSF COMET Consortium authors are listed in the acknowledgements

Word count: 10 526, abstract: 207 words
Tables/figures: 7 figures, 1 table, 7 supplemental figures, 1 supplemental table

Conflict of interest statement

J.A.H., H.S., J.V.H., C.O., L.O., X.G., N.W., A.Q., D.C., A.C, D.F.C., T.R, J.M.M., F.C., A.T., M.B., L.T., A.R., S.B.K., R.N.B., and C.M.R. were employees of Genentech, Inc. at the time of this study and own equity in Roche. The COMET study was supported in part by Genentech funding. C.J.Y. is a Scientific Advisory Board member for and holds equity in Related Sciences and ImmunAI, a consultant for and holds equity in Maze Therapeutics, and a consultant for TReX Bio. C.J.Y. has received research support from Chan Zuckerberg Initiative, Chan Zuckerberg Biohub, and Genentech. C.S.C. has received research funding from Roche-Genentech for an unrelated project as well as from NIH, DOD, and Quantum Leap Healthcare Collaborative. C.S.C. is a consultant for Vasomune, Quark, and Gen1e Life Sciences. C.H. is a consultant for Spring Discovery but does not have any financial interest in the company nor is the work related to what is covered in this manuscript. AR is a co-founder and equity holder of Celsius Therapeutics, an equity holder in Immunitas Therapeutics and, until 31 July 2020, was a scientific advisory board member of ThermoFisher Scientific, Syros Pharmaceuticals, Asimov and Neogene Therapeutics. AR is a named inventor on multiple patents related to single cell and spatial genomics filed by or issued to the Broad Institute.

46 **Abstract**

47 Altered myeloid inflammation and lymphopenia are hallmarks of severe infections, including with
48 SARS-CoV-2. Here, we identified a gene program, defined by correlation with EN-RAGE
49 (*S100A12*) gene expression, which was up-regulated in airway and blood myeloid cells from
50 COVID-19 patients. The EN-RAGE program was expressed in 7 cohorts and observed in patients
51 with both COVID-19 and acute respiratory distress syndrome (ARDS) from other causes. This
52 program was associated with greater clinical severity and predicted future mechanical ventilation
53 and death. EN-RAGE^{+} myeloid cells express features consistent with suppressor cell functionality,
54 with low HLA-DR and high PD-L1 surface expression and higher expression of T cell-suppressive
55 genes. Sustained EN-RAGE signature expression in airway and blood myeloid cells correlated
56 with clinical severity and increasing expression of T cell exhaustion markers, such as PD-1. IL-6
57 treatment of monocytes *in vitro* upregulated many of the severity-associated genes in the EN-
58 RAGE gene program, along with potential mediators of T cell suppression, such as IL-10.
59 Blockade of IL-6 signaling by tocilizumab in a placebo-controlled clinical trial led to a rapid
60 normalization of ENRAGE and T cell gene expression. This identifies IL-6 as a key driver of
61 myeloid dysregulation associated with worse clinical outcomes in COVID-19 patients and
62 provides insights into shared pathophysiological mechanisms in non-COVID-19 ARDS.

63 **Introduction**

64 Altered myeloid cell expression states, including the accumulation of cells with hallmarks of
65 myeloid-derived suppressor cells (MDSC), are consistent features in the blood of COVID-19
66 patients, and serve as a hallmark of severity [1–18]. Monocytes and granulocytes associated with
67 increased COVID-19 severity exhibit low expression of HLA-DR, and high expression of hallmark
68 MDSC genes such as *S100A12* (EN-RAGE), and can impair T cell activation via contact-
69 dependent (i.e., PD-L1) and soluble mechanisms, including IL-10, TGF-β, arginase 1, IDO-
70 dependent tryptophan metabolism, and reactive oxygen and nitrogen species (reviewed in [19–22]).
71 Presence of MDSCs in severe COVID-19 patients, and patients with other severe infections,
72 correlates with reduced T cell numbers, and can impair T cell proliferation and IFN-γ production
73 *ex vivo* [23–28]. Reduced T cell proliferation and tissue sequestration can in turn contribute to the
74 lymphopenia observed in COVID-19 patients with severe disease, which increases with the
75 severity of respiratory failure and is prognostic for higher mortality[29]. Thus, understanding the role
76 of myeloid suppressor cells and the pathways leading to their dysregulation is of critical
77 importance in COVID-19 and other infections.

78

79 The pathways driving myeloid inflammation and the mechanistic connection of maladaptive
80 cellular programs to severe disease and response to drug interventions are not yet understood. IL-
81 6 is a key regulator of inflammation and has been proposed as a potential driver of dysfunctional
82 myeloid immune response in cancer, COVID-19, and other diseases [10,12,20,26,30–33]. IL-6 treatment
83 *in vitro* leads to differentiation of hematopoietic stem cells into $CD14^+$ monocytes expressing a
84 similar expression program to that observed in COVID-19 patient monocytes, including high
85 expression of EN-RAGE and low expression of HLA-DR[10]. Circulating IL-6 levels positively

86 correlate with this severity-associated myeloid state in COVID-19 and other severe infections[10]. It
87 has been suggested that treatment with IL-6-blocking antibodies normalizes alterations in the
88 myeloid compartment that are associated with disease severity[12], a hypothesis requiring placebo-
89 controlled trials to test. Samples from hospitalized COVID-19 patients treated with tocilizumab (a
90 monoclonal antibody against IL6R/Actemra) in a placebo-controlled study (COVACTA, n=438
91 hospitalized COVID-19 patients with hypoxemia randomized 2:1 tocilizumab:placebo) provided
92 a unique opportunity to evaluate the role of IL-6 in shaping myeloid inflammation in patients[34]. A
93 meta-analysis by the World Health Organization concluded that IL-6 antagonists reduce 28-day
94 mortality in patients hospitalized for COVID-19[35].
95
96 Here, we used single cell RNA-seq (scRNA-seq) of peripheral blood mononuclear cells (PBMCs)
97 and bronchoalveolar lavage (BAL) fluid cells collected from COVID-19 patients, to identify a
98 myeloid cell program shared across tissue compartments, defined by high expression of the EN-
99 RAGE gene, among other inflammatory markers. Expression of this program was associated with
100 more severe disease in our discovery cohorts. We replicated this finding using data from the
101 COMET observational study, which includes sampling from endotracheal aspirates (ETA), whole
102 blood, and PBMCs [2,36,37] of COVID-19 patients. Combined single cell profiling of RNA and cell
103 surface proteins (CITE-seq) characterized the immunosuppressive expression program in EN-
104 RAGE signature expressing cells and connected it to cell surface phenotypes of impaired myeloid
105 antigen presentation and T cell exhaustion. The EN-RAGE expression program was associated
106 with several measures of COVID-19 clinical severity and outcomes and was also observed in
107 patients with acute respiratory distress syndrome (ARDS) from other causes, identifying a
108 targetable pathway relevant to ARDS. Finally, blocking IL-6 signaling using tocilizumab in an

109 interventional setting reduced expression of the EN-RAGE signature and normalized T cell
110 numbers in COVID-19 patients from the COVACTA trial, providing mechanistic insight into the
111 therapeutic response to COVID-19 patients to IL-6 blockade.
112

113 **Results**

114 ***A pan-myeloid EN-RAGE signature in blood and airway samples is associated with severe***
115 ***COVID-19***

116 We used publicly available scRNA-seq data from COVID-19 patients to define a gene program
117 that classifies a shared myeloid state across airway and blood samples. We seeded the program by
118 the expression of the gene encoding EN-RAGE (*S100A12*), which has been implicated in several
119 myeloid populations in the peripheral blood associated with COVID-19 severity[2,10,38,39]. EN-
120 RAGE expression is upregulated by IL-6[40], is elevated in the airways of ARDS patients as well as
121 other lung diseases[41], and serum levels correlate with COVID-19 severity[1,4]. We identified a set of
122 84 genes that co-vary (Pearson's $r > 0.5$) with EN-RAGE expression across myeloid cells from
123 bronchoalveolar lavage (BAL) fluid and PBMCs from COVID-19 patients[7,11] (**Fig. 1A**; **table S1**).
124 This gene program showed strong coordinated expression across airway and blood samples and
125 predominant expression in many myeloid cell types (monocytes, neutrophils, and macrophages),
126 although dendritic cells (DCs) and non-classical monocytes showed lower overall expression (**fig.**
127 **S1**). Increased expression of the EN-RAGE program in neutrophil, monocyte and macrophage
128 subsets was associated with greater clinical severity in both blood and airway samples (**Fig. 1B**
129 and **fig. S1C**).
130

131 The EN-RAGE program scores correlated with the scores of a previously-defined MS1 gene set [9],
132 which was associated with increased severity in COVID-19 and sepsis patients[9,10] (Spearman's
133 ρ=0.64 and 0.95 in pseudobulk expression profiles of blood and airway monocytes and neutrophils
134 (5 cohorts) and ρ=0.65 in whole lung myeloid cells (one cohort) (all $p<0.0001$)). Only seven genes
135 (CLU, CYP1B1, LILRA5, NAMPT, S100A12, S100A8, VCAN) are shared between the 84 genes
136 in the EN-RAGE program and the 23 genes in the MS1 signature identified in COVID-19
137 patients[10], which is a significant overlap (p-value=7e-14, hypergeometric test). EN-RAGE
138 program expression was more highly intercorrelated than the MS1 signature across sample types
139 (**Fig. S2A)**. While MS1 had strong pairwise correlations in PBMC myeloid cells, many genes were
140 no longer correlated when measured in whole blood (WB) or endotracheal aspirate (ETA) (**Fig.**
141 **S2B-M)**. Because of the reduced performance of MS1 outside of PBMCs, we used the EN-RAGE
142 program (denoted EN-RAGE$^+$) in subsequent analyses to more specifically evaluate myeloid cells
143 in bulk RNA-seq from whole blood and airway samples, which have greater cellular complexity
144 than PBMC samples.
145

146 ***EN-RAGE signature is associated with acute lung injury from diverse causes***

147 We next hypothesized that the EN-RAGE myeloid program may also be a feature of non-COVID-
148 19 lung injury. To test this hypothesis, we scored the EN-RAGE program in samples from the
149 COMET observational cohort, where 75 patients with either COVID-19 or acute lung injury from
150 other causes were followed longitudinally (Table 1, patient characteristics)[2,36,37]. Whole blood
151 (WB), PBMC, and endotracheal aspirates (ETA) were sampled and profiled by scRNA-Seq. This
152 cohort offers rich clinical and molecular phenotyping to allow single-cell dissection of the
153 connection between the airways and the blood at the mRNA and protein level, and how this relates

154 to clinical outcomes. EN-RAGE signature expression was highest in monocytes, macrophages,
155 and neutrophils, consistent with our previous analyses (**Fig. 2** and **fig. S2**). EN-RAGE$^+$ myeloid
156 cells were present in the blood and airways in both COVID-19 and non-COVID-19 acute lung
157 injury patients, highlighting the generality of this program (**Fig. 2C**).
158

159 ***EN-RAGE signature expression correlates with clinical severity and is prognostic for worse***
160 ***clinical outcomes***

161 In COVID-19 patients, EN-RAGE$^+$ myeloid cells were associated with increased clinical severity
162 at presentation, as defined by the extent of respiratory support required at study enrollment, in
163 monocytes (PBMC) and neutrophils (whole blood) (**Fig. 2** and **fig. S3**). The severity association
164 of monocyte ENRAGE score observed in PBMC was not observed in the smaller number of
165 samples available from whole blood. An association with severity is not found in ETA samples,
166 perhaps since this sample type is only obtained from critically ill patients on mechanical ventilation
167 and so a milder severity group is lacking.
168

169 We next asked whether higher EN-RAGE signature expression predicts worse patient outcomes.
170 In PBMC samples from COVID-19 and non-COVID-19 patients at COMET study enrollment, the
171 EN-RAGE program score was associated not only with greater baseline clinical severity (NIH
172 COVID-19 severity ordinal score) but also worse clinical outcomes (ICU admission and maximal
173 NIH ordinal scale: ≥0.30 p=0.02) (**Fig. 3A** and **fig. S3A-C**). However, these associations were no
174 longer significant once baseline severity measures were considered in our analyses, possibly
175 because of the limited numbers of patients in this cohort and the increased risk of severe outcomes
176 in patients presenting with greater severity. EN-RAGE program expression was not significantly

177 associated with age (Spearman ρ=-0.02, p=0.88) nor with days from symptom onset to study
178 enrollment (Spearman ρ=0.09, p=0.57). EN-RAGE score was higher in patients who presented
179 with or later developed ARDS compared with those who did not by either AECC or Berlin
180 diagnostic criteria ($p<0.01$ for AECC definition, $p<0.05$ for Berlin definition) (**fig. S3D-E**).
181 ENRAGE score was higher in ARDS (AECC definition) resulting from SARS-CoV-2 infection or
182 other etiology ($p<0.05$) (**Fig. 3B**), but the difference in the smaller patient subgroups was not
183 significant when using the more stringent Berlin ARDS definition (**fig. S3F**).
184

185 Leveraging the availability of longitudinal samples from ventilated patients in the COMET cohort,
186 there was a significant association between the temporal trajectory of airway EN-RAGE
187 expression in each patient and patient outcomes (**Fig. 3C).** To test this, we stratified patients into
188 two groups by the number of ventilator-free days (VFD) and compared the slope of the regression
189 lines of the two groups. Airway EN-RAGE expression decreased over time in survivors with
190 fewest days of ventilation and increased in patients who died or had ≥28 days of ventilation
191 ($p<0.05$ linear mixed model, ETA, **Fig. 3C**). Worse clinical outcomes are accompanied by
192 sustained elevated airway levels of EN-RAGE$^+$ cells as well as higher baseline levels in the blood.
193

194 ***EN-RAGE program expression in myeloid cells is associated with increased markers of***
195 ***immunosuppression in blood and airways***

196 The EN-RAGE program score was also associated with expression of genes characteristic of
197 MDSCs, suggesting one path through which EN-RAGE$^+$ cells may contribute to clinical severity.
198 Specifically, EN-RAGE program expression was correlated with metrics of suppressed myeloid
199 and lymphoid states across another five COVID-19 cohorts[2,5,7,11,12,36,37], spanning ETA, BAL,

200 lung, PBMC, and blood samples (complete results in **table S2**). For example, in COMET PBMC
201 monocytes, EN-RAGE program expression correlated with high *CD14* (Spearman ρ=0.65,
202 p<0.001), *CCR2* (ρ=0.25, p<0.05) and *PTGER2* (ρ=0.38, p<0.001) (**Fig. 3D**). *CCR2* and *PTGER2*
203 are two receptors important for myeloid cell recruitment to the infected lung via *CCL2* and
204 prostaglandins, respectively. EN-RAGE program expression correlated with low expression of
205 MHC class II genes, suggesting reduced capacity for antigen presentation (*HLADRA:* ρ=-0.45 and
206 *HLADRB1:* ρ=-0.48, p<0.001, **Fig. 3D** and **table S2**). In blood monocytes, there was a positive
207 correlation with *STAT3*, a key transcription factor regulating MDSC gene expression (ρ=0.79,
208 p<0.001, **Fig. 3D**). MDSCs can suppress T cells using context-specific mechanisms across sites of
209 infection or malignancy, and the mechanisms used can also differ depending on whether they
210 originate from the monocytic or granulocytic lineage[13,20]. In blood monocytes, EN-RAGE program
211 expression was positively correlated with expression of genes encoding effectors that can suppress
212 T cells through reactive oxygen species (*CYBB/PHOX*) and prostaglandins (*PTGER2*), and
213 *TGFβ1*, but inconsistent associations with arginase (*ARG1*) and tryptophan depletion (*IDO1*)
214 across cohorts (**Fig. 3D** and **table S2**). Granulocytic EN-RAGE$^+$ cells had similar associations as
215 their monocytic counterparts, with notable differences including stronger correlations with *PDL1*
216 and *TGFβ1* and little to no association with reactive oxygen species (*CYBB/PHOX*) and *PTGER2*
217 compared with EN-RAGE$^+$ monocytes (**Fig. 3D** and **table S2**). Consistent with MDSCs
218 characterized in other infections and cancers[20,22,42], EN-RAGE$^+$ cells expressed higher levels of
219 multiple potential mediators of immunosuppression (*PDL1*, *CYBB/PHOX*, and *TGFβ1*) with some
220 genes preferentially expressed by monocytic lineages (i.e. *CYBB/PHOX* ρ>0.4, **table S2**) or
221 granulocytic lineages (i.e. *TGFβ1* ρ>0.6, **table S2**) (**table S2**). EN-RAGE program expression in
222 PBMC myeloid cells was modestly correlated with plasma protein levels of IL-6, a potential driver

223 of MDSCs, and IL-10, a potential mediator of T cell suppression (Spearman ρ=0.41, p=0.005 and
224 ρ=0.29, p=0.05, respectively; **Fig. 3E**).
225

226 These associations were also largely observed in airways samples, suggesting an overall consistent
227 phenotype in both the blood and the infected lung (**Fig. 3D**). As in the blood, EN-RAGE program
228 expression in monocytes and neutrophils was positively correlated with*, STAT3* in ETA samples
229 but lacked the correlations with *CCR2* and *HLADR*, showed stronger correlations with *CCR5*, and
230 inconsistent relationships with *CYBB* and *CD14* (**Fig. 3D** and **table S2**). EN-RAGE^{+} monocytes
231 and neutrophils cells in lung and airway samples (ETA, BAL, and lung post-mortem autopsy
232 tissue) had increased association with *PDL1*, *IL10, TGFβ, IDO,* and *IL1β*, which can suppress T
233 cell function, compared to the blood (**Fig. 3D,F** and **table S2**). Peripheral blood myeloid cells
234 expressed lower levels of *IL10* and *IL1β* and had weaker correlation with the EN-RAGE signature
235 when transcripts were detected, illustrating the importance of sampling infected tissues and
236 establishing blood correlates of tissue immune responses (**Fig. 3D** and **table S2**). Across four
237 patient cohorts, airway EN-RAGE^{+} monocytes and neutrophils consistently expressed multiple
238 markers of inflammation with autoregulatory functions that can be immunosuppressive, including
239 *IL10, PDL1, TGFβ1, IL1β*, and *IDO* (**table S2**).
240

241 **Characterization of EN-RAGE^{+} myeloid and T cell phenotypes**

242 To connect the EN-RAGE expression program to cellular phenotypes, we used CITE-seq data
243 from PBMCs in COMET to relate cell surface protein expression and EN-RAGE program
244 expression. The EN-RAGE signature was most highly expressed in CD14^{+}CD16^{lo}HLA-DR^{lo}
245 classical monocytes (cM) (**Fig. 4A-B**), confirming the reduced antigen presentation capacity

246 suggested by scRNA-seq data (**table S2**). EN-RAGE signature scores on cMs positively correlated
247 across patients with cM surface expression of 19 of the 188 CITE-Seq measured proteins
248 (FDR<0.05, **Fig. 4C**), including three markers characteristic of MDSCs: PD-L1 (CD274,
249 Spearman ρ=0.43, FDR=0.008), podoplanin (PDPN, ρ=0.52, FDR=0.001), and CD38 (ρ=0.49,
250 FDR=0.002), which is IL-6-inducible in tumors[43,44]. Conversely, EN-RAGE signature scores on
251 cM were negatively correlated with 19 markers (FDR<0.05, **Fig. 4C**), including HLA-DR (ρ=-
252 0.73, FDR<0.0001), the T cell costimulatory protein CD40L (ρ=-0.36, FDR=0.03), the LFA
253 subunit CD11A involved in trafficking and activation (ITGAL, ρ=-0.52, FDR=0.002), and two
254 markers of granulocytic MDSCs (SIGLEC7: ρ=-0.52, FDR 0.001; CD244: ρ=-0.50, FDR=0.002)
255 (**Fig. 4C**).
256

257 EN-RAGE program scores in cMs also negatively correlated with the level of the activation marker
258 CD40 on $CD4^+$ T cells (**Fig. 4D**), consistent with the negative correlation of the expression of
259 ligand CD40L on cMs with their EN-RAGE program (**Fig. 4C**). Conversely, EN-RAGE program
260 scores in cMs were positively correlated with three proteins expressed by exhausted $CD4^+$ and
261 $CD8^+$ T cells: podoplanin/PDPN (Spearman ρ=0.37, FDR=0.04), CX3CR1 (ρ=0.51, p≤0.01) and
262 TNFSF14/LIGHT (ρ=0.39, p=0.03) (**Fig. 4D-E**). These data support the EN-RAGE program
263 activity in cMs correlating with distinct $CD8^+$ and $CD4^+$ T lymphocytes activation states across
264 patients.
265

266 Moreover, the dynamic changes in EN-RAGE program expression and markers of myeloid
267 activation and T cell exhaustion were associated with clinical outcomes. Patients with PBMC
268 CITE-seq data were categorized into 4 outcome groups based on survival and the duration of

269 mechanical ventilation. In monocytes from patients with more severe outcomes compared with
270 patients not requiring ventilation, HLA-DR trended lower than healthy (indicated by red line) and
271 failed to recover to healthy levels over 14 days (**Fig. 4F**), and trends of sustained higher PD-L1
272 and EN-RAGE score in some greater severity groups remained higher in ventilated patients (**Fig.**
273 **4G-H**). On $CD8^+$ and $CD4^+$ T cells, T cell exhaustion markers (PD-1, LAG3, TIGIT, CTLA4, and
274 BTLA4) showed greater increases over 14 days in patients with worsening outcomes (>7 days
275 mechanical ventilation and/or death) compared with non-ventilated patients (**Fig. 4I-L** and **fig. S4**,
276 Pearson correlation $p<0.05$, not significant for PD-1 on $CD4^+$ T cells). Therefore, the EN-RAGE
277 myeloid expression program correlates with markers of a suppressive cell surface phenotype on
278 monocytes, and with reduced activation of $CD4^+$ and $CD8^+$ T cells, as indicated by increasing
279 expression of T cell exhaustion markers over time (**Fig. 4I-L** and **fig. S4**).
280

281 ***IL-6 induces the EN-RAGE program in monocytes in vitro***

282 Several lines of evidence led us to hypothesize that IL-6 can be a regulator of the EN-RAGE
283 program. First, IL-6 treatment of HSPCs promotes upregulation of the MS1 gene signature in
284 monocytes[10], which correlates with the EN-RAGE program (Spearman $\rho \geq 0.64$ in monocytes,
285 $p<0.0001$ across 5 cohorts as described above). Moreover, blood monocyte EN-RAGE program
286 expression correlates with plasma IL-6 protein levels, and with levels of monocyte *STAT3* mRNA,
287 a transcription factor activated by IL-6 signaling (**Fig. 3D-E** and **table S2**). To test this hypothesis,
288 we treated human primary monocytes with IL-6 *in vitro* followed by RNA-seq.
289

290 IL-6 treatment altered the expression of 36 of 84 EN-RAGE program genes (Benjamini-Hochberg
291 FDR<0.05, **Fig. 5A**), as well as of *IL10, IL1β, CYBB*, and *CCR2* (**fig. S5**), all features of EN-

292 RAGE$^+$ monocytes in COVID-19 patients (**Fig. 3D**). Using gene set enrichment analysis, we found
293 that IL-6 could potently up-regulate the expression of EN-RAGE and MS1 signature genes
294 (Benjamini-Hochberg adjusted $p<0.001$ and $p<0.01$, respectively; **Fig. 5B**). Our data suggest that
295 IL-6 is sufficient to induce an expression program in monocytes *in vitro* that is similar to the EN-
296 RAGE$^+$ program associated with severity and with markers of a T cell suppressive phenotype in
297 patients.
298

299 ***The myeloid EN-RAGE program correlates with expression programs of suppressive myeloid***
300 ***cells and impaired T cells and with increased clinical severity in an interventional COVID-19***
301 ***clinical trial***

302 We next asked if blocking IL-6 signaling in patients correlated with a change in EN-RAGE
303 program expression, leveraging data from COVACTA, a double-blind randomized clinical trial of
304 tocilizumab (anti-IL6R/Actemra) in hospitalized COVID-19 patients with hypoxemia[34].
305 Consistent with our findings in other cohorts, bulk RNA-seq expression profiles from whole blood
306 collected at baseline from 438 patients showed higher normalized enrichment scores for the EN-
307 RAGE program in patients requiring positive pressure ventilation at baseline compared with those
308 who did not (**Fig. 6A-B,** FGSEA Benjamini-Hochberg FDR < 0.05). The EN-RAGE gene set was
309 also enriched in patients needing future mechanical ventilation or progressing to death even when
310 controlling for the association with baseline severity (**Fig. 6C-D**, FGSEA Benjamini-Hochberg
311 FDR<0.05). The prognostic relationship of the ENRAGE signature with mortality was maintained
312 even when adjusting for myeloid cell proportions in blood (**fig. S6A-E**; FDR<0.05, FGSEA).
313 Moreover, lower expression of gene sets classifying CD8$^+$ and CD4$^+$ T lymphocytes
314 (CIBERSORT[45]) was associated with worse clinical severity and outcomes (**Fig. 6B-D**,

315 (Benjamini-Hochberg FDR<0.05). Furthermore, consistent with COMET whole blood scRNA-
316 seq, EN-RAGE program scores were positively correlated with expression of *PDL1, IL10,* and
317 *IL1β* in whole blood at day 1 in COVACTA patients (**Fig. 7A**), as well as with serum protein levels
318 of EN-RAGE, IL-6, IL-10, IL-1β, and ARG1 (**fig. S8A**, t-test p<0.05). Examination of T cell genes
319 that were associated with EN-RAGE program expression in scRNA-seq data (**Fig. 7A**) revealed
320 that high myeloid EN-RAGE program expression in COVACTA bulk RNA-seq was associated
321 with low expression of T cell effectors (granzyme, perforin and lymphotoxin (*GZMB, GZMM,*
322 *PRF1, LTA*)), cytotoxicity (*FASL*), and *IFNG*), activation markers (*KLRK1/NKG2D*) and
323 exhaustion markers (*CTLA4, LAG3, CD160*). Many of these genes were expressed at a lower level
324 in patients with more severe disease (*IFNG*, *FASLG, CTLA4, LAG3, TIGIT, TBX21/Tbet, XCL1*;
325 **Fig. 7B**, Benjamini-Hochberg FDR<0.05 and fold change < $\log_2$ -0.5). Higher EN-RAGE program
326 expression was also correlated with lower lymphocytes (ρ=-0.5) and monocytes (ρ=-0.2) and
327 increased neutrophils (ρ=0.5) (**fig. S8A**, all p<0.001). Thus, the COVACTA cohort shows similar
328 features to those observed in COMET, including the expression of the EN-RAGE$^+$ myeloid
329 program and its correlation with greater clinical severity and worse clinical outcomes.
330

331 ***IL-6 blockade decreases the myeloid EN-RAGE state and increases T cells in COVID-19***
332 ***patients***

333 Finally, to understand the role of IL-6 in patients, we examined the effect of tocilizumab treatment
334 on the EN-RAGE myeloid state in COVID-19 patients and effect on T cells using longitudinal
335 samples from the COVACTA study[14,34]. Blockade of IL-6 signaling reduced expression of the EN-
336 RAGE program and increased T cell signature expression after 3 or 7 days of tocilizumab treatment
337 compared with placebo (**Fig. 6A, E**; Benjamini-Hochberg FDR<0.05). Consistent with the EN-

338 RAGE program expression, MDSC and MS1 signatures were elevated in patients with worse
339 baseline clinical severity and needing future mechanical ventilation or who died, and decreased
340 following tocilizumab treatment (**Fig. 6B-E**, Benjamini-Hochberg FDR<0.05). These enrichments
341 were consistently maintained when adjusted for blood cell type composition (proportion of total
342 leukocyte levels added as covariates to the DESeq2 model) (**fig. S6A-C**). The effect of tocilizumab
343 on gene set enrichment was comparable between tertiles of baseline serum IL-6 protein levels (**fig.**
344 **S6D-E**). EN-RAGE program gene expression was sustained over the first 7 days in patients with
345 worse clinical outcomes at day 28 (hospitalized or non-survivor vs discharged, **Fig. 6F**). The
346 ENRAGE program was reduced following tocilizumab treatment more than in placebo treatment
347 over the first 7 days, particularly in patients with better clinical outcomes (**Fig. 6F** and **fig. S7A**).
348 At the same time, CD8 T cell-associated gene expression rapidly increased after tocilizumab
349 treatment, again particularly in patients that showed clinical improvement (**Fig. 6F** and **Fig. 7C**).
350 Similar results were observed for the MS1 severity-associated myeloid and CIBERSORT $CD4^+$ T
351 cell gene sets (**fig. S7B, D**). This corresponded with a more rapid increase in blood lymphocytes
352 and decrease in neutrophil cell counts in tocilizumab-treated patients who were discharged by 28
353 days compared with placebo (**fig. S7E-J**). When we compared the change between day 7 and 1 in
354 EN-RAGE program expression with the change in measured blood cellularity, patients with a
355 greater decrease in EN-RAGE had a greater increase in blood lymphocytes and monocytes and
356 decreases in neutrophils (**fig. S8B-D**). This was more pronounced in patients treated with
357 tocilizumab compared with placebo.
358

359 The reduction in EN-RAGE program following IL-6 blockade corresponded with normalization
360 of potential mediators and correlates of T cell suppression. Patients with a greater decrease in EN-

361 RAGE program expression from day 1 to 7 had greater decreases in serum EN-RAGE, IL-10, IL-
362 1β, and ARG1 protein levels, as indicated by a positive slope of the correlation line (**fig. S8E-H**).
363 IL-6R blockade with tocilizumab resulted in a greater decrease in ENRAGE program expression,
364 as indicated by a greater offset in the regression in the tocilizumab-treated arm compared with
365 placebo, and a greater decrease in this set of serum proteins, as indicated by more green vs red dots
366 in the bottom left quadrant (**fig. S8E-H**). This correlated with increased expression of the T cell
367 genes *IFNG, FASLG, CTLA4* and *XCL1* in tocilizumab-treated patients (**Fig. 7C**). In sum,
368 blockade of IL-6 signaling in COVID-19 patients rapidly normalizes the severity-associated
369 myeloid and T cell states, identified using both patient scRNA-seq data and the IL-6 *in vitro* model,
370 to levels in healthy individuals, which correlates with clinical improvement by 28 days.
371

372 **Discussion**
373

374 While altered myeloid states are hallmarks of COVID-19 disease severity[1–18], the pathways
375 driving maladaptive myeloid inflammation have not been clearly defined. This study supports a
376 working model whereby IL-6 differentiates myeloid cells from both monocytic and granulocytic
377 lineages to a suppressive phenotype characterized by low antigen presentation on HLA-DR and
378 increased expression of multiple factors that can suppress T cells (IL-10, PD-L1, TGF-β1) (**Fig.**
379 **7D**). We define a pan-myeloid ENRAGE program of coordinately-expressed genes in the airways
380 and blood of COVID-19 patients that is prognostic for severe outcomes and is robust across 7
381 cohorts[2,5–7,11,12,14,36,37]. EN-RAGE^{+} cells express multiple phenotypic hallmarks of MDSCs by cell
382 surface protein analysis: decreased capacity for antigen presentation and co-stimulation through
383 HLA-DR and CD40, and increased potential to suppress T cells through PD-L1. This was
384 associated with sustained elevated expression of exhaustion markers on T cells such as PD-1 in

385 patients with prolonged mechanical ventilation or who died. COVID-19 patients with higher EN-
386 RAGE signature expression had a greater risk of future mechanical ventilation and mortality, and
387 EN-RAGE^{+} myeloid cell impairment of optimal T cell-mediated immunity is one potential
388 mechanism. Therapeutic blockade of IL-6 signaling with tocilizumab is sufficient to attenuate
389 expression of the EN-RAGE signature in blood cells and normalize T cell numbers, correlating
390 with clinical improvement. While COVACTA did not meet the primary endpoint of improving
391 clinical status on day 28, tocilizumab demonstrated clinically meaningful benefits, such as
392 shortening hospital stay by 8 days, compared with the placebo arm[34]. Importantly, IL-6 antagonists
393 significantly reduced mortality compared with usual care in a large meta-analysis using data from
394 27 trials[35]. Sepsis patient serum promotes expression of this severity-associated program in an IL-
395 6R-dependent manner using an *in vitro* system[10]. These data demonstrate the importance of IL-6
396 in altering immune cell phenotypes in COVID-19 patients and provide a potential mechanism for
397 the therapeutic benefit of tocilizumab in patients hospitalized with COVID-19[35].

398 COVID-19 patients with lymphopenia are at higher risk for worse clinical outcomes in the
399 COVACTA cohort[29]. In addition to being reduced in numbers, suppressed T cell phenotypes have
400 been described in severe COVID-19 patients. Polyfunctional Th1 and Th17 CD4^{+} and CD8^{+} cell
401 subsets are underrepresented in SARS-CoV-2 infection, with less proliferation and impaired IFN-
402 γ and IL-2 secretion following restimulation *in vitro*[46,47]. T cells with increased expression of
403 activation (OX40, CD69) and exhaustion (PD-1, TIGIT, TIM1) markers have been observed in
404 some[38,48] but not all cohorts[49] and functional exhaustion of CD8^{+} T cells has been reported[50–52]. In
405 single cell analysis of the COMET cohort, a phenotype of sustained elevated expression of PD-1,
406 TIGIT, and LAG3 was observed on T cells in patients requiring longer mechanical ventilation and
407 non-survivors. As tocilizumab increased the number of circulating T cells, the observed increase

408 in markers of T cell function such as IFNγ and CD69 may result from increased T cell abundance
409 rather than increased functionality per cell. Differential regulation of T cell genes suggests a
410 potential effect of tocilizumab on T cell quality in addition to quantity. IL-6R blockade increases
411 markers of early polyfunctional T cells (*IFNG, XCL1, CD69*) and recently activated/less exhausted
412 cells (*IL7R*) while markers associated with broader spectrum of T cell functional states (i.e.
413 cytotoxic T cell markers T-bet (*TBX21*), perforin (*PRF1*), and granzymes (*GZMM, GZMB*)) are
414 less affected. However, there is limited ability to infer T cell functionality from bulk RNA-seq
415 data. Future studies using multi-dimensional flow cytometry data will enable more precise
416 definition of how IL-6 alters the T cell phenotype in COVID-19, both via myeloid activation and
417 acting directly on T cells. NK cells are important antiviral effector cells that can be suppressed by
418 MDSCs[19] and can express exhaustion markers[49]. A potential connection between EN-RAGE+
419 myeloid cells and NK cells or the suppressive regulatory T cell phenotype observed in severe
420 COVID-19 patients[53] remains to be characterized.

421 Suppressive myeloid cells are one potential mechanism underlying impaired T cell
422 immunity in severe COVID-19. MDSCs express mediators of T cell suppression in a context-
423 dependent manner, depending on the type of infection or tumor[20,22]. MDSCs express multiple
424 genes through which they may potentially suppress T cells. Moreover, differential correlations
425 between the EN-RAGE signature and genes encoding immunosuppressive mediators were
426 observed between cell lineage (granulocytic vs. monocytic) and compartment (blood vs. airways).
427 MDSCs are often identified by low HLA-DR expression as a marker of impaired antigen
428 presentation capacity[23,26–28,46]. Interestingly, while some features of EN-RAGE^{+} cells were
429 consistent between blood and airways (i.e. high PD-L1), the expression of other genes was tissue-
430 dependent, and the low expression of HLA-DR in the blood was lost in airway samples. This is

431 consistent with the observation that HLA-DR^{lo} MDSCs were not found in ETA airway samples by
432 flow cytometry[26]. These data suggest that EN-RAGE^{+} myeloid cells home to the infected lung and
433 adopt a tissue-specific phenotype, with increasing expression of IL-10 and IDO and decreasing
434 expression of CCR2 and CYBB, highlighting the importance of characterizing immune responses
435 at the site of infection. The EN-RAGE^{+} myeloid state may underlie disease severity through
436 additional mechanisms. For example, EN-RAGE^{+} cells express higher *IL-1β* and *TGF-β1* which
437 can increase endothelial and epithelial cell permeability, respectively, and potential mechanisms
438 whereby EN-RAGE^{+} cells could affect barrier integrity and edema in patients with acute lung
439 injury remains to be explored[10,54,55].

440 This study connects immune cell phenotypes in the blood with the myeloid EN-RAGE
441 state in the airways using paired quantification of mRNA and surface proteins at single cell
442 resolution in PBMCs and ETA single cell transcriptomes from the COMET study and longitudinal
443 blood mRNA expression data from the large Phase 3 COVACTA study. The inclusion of patients
444 with acute lung injury from other causes in the COMET cohort reveals that EN-RAGE^{+} myeloid
445 cells are relevant to insults in addition to SARS-CoV-2 infection, and identifies a targetable
446 pathway relevant to ARDS. IL-6 predicts severe patient outcomes[29] and has been hypothesized to
447 be a driver of myeloid differentiation in severe infections[10,12]. We show that tocilizumab treatment
448 rapidly normalized myeloid and T cell states to healthy control levels, which was correlated with
449 improved clinical outcomes. This study establishes the importance of IL-6 in driving
450 differentiation of the severity-associated EN-RAGE^{+} myeloid state in patients. COVID-19 and
451 cancer share risk factors, such as age and metabolic syndrome, and underlying immunobiology,
452 such as MDSCs and T cell exhaustion, making it appealing to speculate that EN-RAGE^{+} myeloid
453 cells may contribute to pathology in multiple diseases.

454 **Methods**

455 *Reanalysis of published scRNA-seq data*

456 Raw count data from Schulte-Schrepping, *et al.*[11] were downloaded from http://fastgenomics.org.
457 For analysis of the PBMC data collected using 10x Genomics droplet-based capture, and whole
458 blood collected using Rhapsody microwell-based capture, the raw count data was reprocessed
459 using scripts written in the R programming language[56] and packages from the Bioconductor project
460 (https://www.bioconductor.org). Briefly, counts were normalized using the
461 computeLibraryFactors method from the scater R package[57] and dimensionality reduction was
462 performed using PCA followed by UMAP projection. For calculating PCA, the top 5000 most
463 variable genes were selected, accounting for overall expression level using the modelGeneVar
464 method from the scran R package[58]. The UMAP projection was calculated using the first 10
465 principal components. Graph-based clustering was performed using the Louvain algorithm on the
466 same 10 principal components. Marker genes for each cluster were determined using pairwise t-
467 tests, calculated using the pairwiseTTest method from the scran R package, and were used to
468 manually assign broad cell type labels to each cluster. Clusters from the same broad cell type
469 classification were merged. The myeloid populations (monocytes, DCs and neutrophils) were
470 separately re-clustered using the same procedures: the 5000 most variable genes were selected,
471 used for PCA calculation, graph-based clustering and UMAP projection. Marker genes were
472 calculated for each cluster, and clusters were manually assigned using the marker gene lists.

473

474 Raw sequencing reads from Liao, *et al.*[7] were downloaded from SRA (PRJNA608742).
475 Sequencing data were then processed using cellranger v4.0.0 (10x Genomics, Pleasanton, CA,
476 USA) using GRCh38 as the reference genome, and gene models from GENCODE (v27) for

477 assigning reads to genes. The emptyDrops method was used from the DropletUtils R package[59] to
478 identify barcodes that corresponded to cellular droplets. Any barcode with fewer than 200 UMIs
479 or 100 genes detected was removed. This allowed us to retain neutrophil-containing droplets, as
480 these are mostly removed by default processing using cellranger. Droplets with high abundance of
481 mitochondrial RNA (>10%) were removed. This yielded 90592 cells for further analysis. The same
482 procedures described above were used to normalize, cluster and annotate cells into broad
483 populations (macrophage, neutrophil, T cell, epithelial cell, B cell). The myeloid populations
484 (macrophages and neutrophils) were selected and reclustered into more fine-grained populations
485 using the same strategy as above.
486
487 Data from Silvin, et al.[12] were retrieved from the European Genome Archive (EGA) under
488 accession number E-MTAB-9221 as FASTQ files. Sequencing data were processed as detailed
489 above for PRJNA608742, using the same parameters for identifying cellular droplets and filtering
490 droplets with high mitochondrial RNA abundance. Normalization, clustering and manual
491 annotation was performed as described above. Count data from Delorey, et al.[5] were downloaded
492 from the Broad Single Cell Portal using accession number SCP1052. We used the cell annotations
493 as defined within that dataset, selecting cells labeled as Myeloid using the Cluster field defined by
494 the authors. Data from Grant, et al.[6] were retrieved from the Gene Expression Omnibus (GEO)
495 under accession number GSE155249. Normalization and clustering were performed as above.
496 Annotations from the original publication were used to group cells into broad lineages: epithelial
497 cells, B cells, T cells, dendritic cells, mast cells, macrophages and mixed myeloid cells.
498
499 *Pseudobulk expression profile calculation*

500 The aggregateAcrossCells method from the scater R package[57] was used to calculate pseudobulk
501 expression profiles for each cell population in a sample. This method uses the sum of raw counts
502 to determine an estimate of the aggregate expression of that cell type in a sample. The TMM
503 method from the edgeR R package[60] was used to normalize the pseudobulk count data within each
504 dataset. Signature score calculation in pseudo-bulk data was performed as previously described[61]
505 using the GSDecon package (https://github.com/JasonHackney/GSDecon).
506

507 *COMET PBMC CITE-seq analysis*

508 The raw scRNA-seq counts were normalized using the 'LogNormalized' method implemented in
509 the 'NormalizeData' function from the Seurat R package[62]; with this method, the feature counts
510 are divided by the total counts for each cell, multiplied by a scale factor of 10,000, and then natural-
511 log transformed. The raw ADT counts were normalized using the 'CLR' method implemented in
512 Seurat's 'NormalizeData' function; with this method, a centered log ratio transformation is
513 applied. The ENRAGE and MS1 gene set scores were calculated for each cell using the
514 'score_genes' function implemented in the scanpy Python package[63]. All of the pseudobulk values
515 for each cell population in a sample (i.e., sample + cell type)—that is, the mRNA expression, ADT
516 expression, and gene set scores—were calculated as the average across all cells in that population.
517 Correlations between gene set scores and ADT expression were on pseudobulk data and refer to a
518 population of cells across patients.
519

520 *Identification of EN-RAGE gene expression induced by IL-6 in vitro.*

521 PBMCs were isolated from 50 mL of heparinized blood of four healthy donors by Ficoll-Paque.
522 Primary human monocytes were purified from PBMC by Miltenyi Pan Monocyte Isolation Kit and

523 cultured in RPMI with 10% heat-inactivated FBS, 10 mM HEPES and L-glutamine. The primary
524 human monocytes were stimulated with 10 ng/mL IL-6 + 18.7 ng/mL IL6R for 24 hours, and
525 RNA-seq performed on bulk cells. Unsupervised clustering using average linkage cluster
526 difference and Euclidean point distance metrics were used to generate heat maps. RNA was
527 isolated using the Qiagen RNeasy 96 kit (Qiagen catalog: 74182). Total RNA was quantified with
528 Qubit RNA HS Assay Kit (Thermo Fisher Scientific catalog: Q32852) and quality was assessed
529 using RNA ScreenTape on 4200 TapeStation (Agilent Technologies catalog: 5067-5576). cDNA
530 library was generated from 2 nanograms of total RNA using Smart-Seq V4 Ultra Low Input RNA
531 Kit (Takara catalog: 634894). 150 picograms of cDNA was used to make sequencing libraries by
532 Nextera XT DNA Sample Preparation Kit (Illumina catalog: FC-131-1024). Libraries were
533 quantified with Qubit dsDNA HS Assay Kit (Thermo Fisher Scientific catalog: Q32851) and the
534 average library size was determined using D1000 ScreenTape on 4200 TapeStation (Agilent
535 Technologies catalog: 5067-5582). Libraries were pooled and sequenced on the Illumina NovaSeq
536 6000 to generate 30 million single-end 50 base pair reads for each sample. Sequencing reads were
537 filtered and aligned using HTSeqGenie v4.4.2[64]. GSNAP v2013-11-01 was used for alignment,
538 through the HTSeqGenie wrapper, against the GENCODE 27 Basic gene model on the human
539 genome assembly GRCh38. Only reads with unique genomic alignments were analyzed.
540 Normalized CPM (Counts Per Million) were used as a normalized measure of gene expression,
541 calculated using method provided in edgeR[60].
542

543 *COMET cohort*

544 The COVID-19 Multi-Phenotyping for Effective Therapies (COMET) cohort collected PBMCs,
545 whole blood, ETA and plasma longitudinally from hospitalized patients presenting with COVID-

546 19 symptoms. This study included 75 patients with samples collected in 2020, of whom 57 were
547 positive (76%) for SARS-CoV-2, along with 11 healthy controls[2,36,37]. Table 1 summarizes the
548 patient characteristics. All-cause mortality occurred within 30 days for 9 of 10 subjects. Ventilator-
549 free days (VFDS) were assessed at D28, with fatal cases assigned 0. NIH COVID-19 ordinal
550 severity score and Sequential Organ Failure Assessment (SOFA) scores were assessed at study
551 enrollment (Day 0), when baseline samples were collected, with a 9 day median time from
552 symptom onset (4-13 IQR). Severity groups were defined as follows. PBMC: Moderate = no
553 supplemental O_2, severe = supplemental O_2 and critical = mechanical ventilation. Whole blood:
554 Mild/Moderate = 0 days on ventilator and no more than 1 day in ICU, Severe patients had ≥1 day
555 on ventilator. ETA: Critical=VFDS=0 (ventilation for ≥28 days or death), severe ETA=VFDS>0.
556

557 PBMCs were isolated and single cell RNA sequencing and Cellular Indexing of Transcriptomes
558 and Epitopes by Sequencing (CITE-seq) data was generated as previously described[37], with the
559 complete protocol available on protocols.io (https://www.protocols.io/view/10x-citeseq-protocol-
560 covid-19-patient-samples-tetr-bqnqmvdw). Data was generated for 188 unique cell surface
561 antigens. CITE-seq data was included from 128 samples collected at day 0, day 7 and/or day 14
562 from 60 patients. Single cell RNA-seq data generated from PBMC collected at day 0 from 49
563 patients, whole blood collected at day 0 for 18 patients, and 41 ETA samples collected
564 longitudinally from 16 patients were included in this study. Bulk gene expression data was
565 generated from 182 samples collected longitudinally from 19 patients. Plasma cytokine and paired
566 ETA scRNA-seq data was available for only 7 samples, precluding correlation analyses.
567

568 *COVACTA tocilizumab clinical trial*

569 A total of 438 hospitalized COVID-19 patients were randomized 2:1 for anti-interleukin-6 receptor
570 antibody, tocilizumab, or placebo and included in the modified intention to treat population
571 (tocilizumab: 294, placebo: 144). Hospitalized patients were ≥18 years of age with COVID-19
572 pneumonia confirmed by a positive SARS-CoV-2 PCR test and evidenced by x-ray or computed
573 tomography (CT) scan. Eligible patients had a blood oxygen saturation of ≤93% or partial pressure
574 of oxygen/fraction of inspired oxygen of <300 mm/Hg. Details of the COVACTA study design
575 have been published (Clinical trials.gov NCT04320615)[34]. Population demographics for the 404
576 patients with available blood RNA-seq data are described in Table 1.
577

578 Serum IL-6 was quantified using a validated in vitro diagnostic method (Roche Cobas; Roche
579 Diagnostics, Indianapolis, IN) at central laboratories (PPD). Complete blood counts were
580 measured using standard clinical chemistry and haematology methods available at local hospital
581 laboratories. IFNγ and IL10 were measured by qualified immunoassays (Simpleplex,
582 ProteinSimple, San Jose, CA, USA) at central laboratories (Covance). The Olink Explore platform
583 was used to measure 1472 serum proteins (Olink, Uppsala, Sweden). RNA was isolated from blood
584 PaxGene (Qiagen, Hilden Germany) samples by Q2 Solutions. 1.25 ug of RNA was used for
585 generating sequencing libraries with the TruSeq® Stranded mRNA Library Prep kit (Illumina, San
586 Diego, CA, USA). The libraries were sequenced by Illumina NovaSeq by 50 bp single-end reads
587 at a read depth of 50 million reads per sample.
588

589 For the time point comparisons (D1 to D7) patients were subset to those subjects with
590 measurements at both time points before differential expression analysis with DESeq2. Unfiltered
591 DESeq2 outputs were ranked by log2 fold change and then the FGSEA Bioconductor package was

592 used to calculate enrichment scores. We used the ggplot2 package to generate visualizations. T
593 cell genes with a relationship to EN-RAGE state in COMET scRNA-seq data were examined in
594 COVACTA, and limited to the subset of T cell suppressive genes that were predominantly
595 expressed by T cells in COMET whole blood transcriptome data to permit analysis of bulk gene
596 expression data. Computational methods are described in more detail elsewhere[14].
597

598 *COVID-19 clinical severity*

599 Within the COVACTA clinical trial, the NIH COVID-19 ordinal severity scale was used to assess
600 disease severity: 3=hospitalized not requiring supplemental O_2, 4= supplemental O_2, 5= non-
601 invasive/high flow O_2, 6= mechanical ventilation, 7= mechanical ventilation + additional organ
602 support (eg, vasopressors, renal replacement therapy, ECMO), 8=death. In the COMET cohort of
603 PBMC samples, moderate = no supplemental O_2 (NIH ordinal scale 3-4), severe = supplemental
604 O_2 (5-6) and critical = mechanical ventilation (7). The maximal NIH ordinal severity scale recorded
605 during hospitalization was calculated for each patient in COMET. Ventilator-free days were
606 calculated over 28 days, with fatal patients scored as 0. ARDS was diagnosed using the American-
607 European Consensus Conference (AECC) definition[65] or Berlin definition[66]. The sequential organ
608 failure assessment (SOFA) score was calculated at study enrollment.
609

610 *Statistical analysis*

611 Gene expression was $\log_2$ normalized. Patient demographics are given as median (IQR) and
612 frequency (%). Medians and first and third quartile ranges are shown in box and whisker plots and
613 medians are shown on dot plots. Longitudinal COVACTA line plots show means and 95%
614 confidence intervals. Two-sided unpaired t-tests were used to compare gene signature scores

between cell types in pseudobulk scRNA-seq data. Student's t-test was used to calculate p values for comparisons of EN-RAGE gene set scores and clinical severity. A mixed linear model was used to compare slopes of longitudinal EN-RAGE gene set expression between severity groups. Spearman correlations and two-tailed p values were calculated to examine relationships between biomarkers and clinical severity and EN-RAGE gene set vs. myeloid gene expression. False discovery rates were calculated for differential expression analysis of bulk RNAseq data (accounting for transcriptome-wide analysis of x genes), GSEA (accounting for the x gene sets analyzed), and COMET PBMC CITE-seq data (accounting for 188 measured proteins), using the Benjamini-Hochberg method. Biorenderer was used to generate some figures.

Study approval

The COMET study was approved by the Institutional Review Board: UCSF Human Research Protection Program (HRPP) IRB# 20-30497 and informed consent was obtained for patients. COVACTA was conducted in accordance with Good Clinical Practice guidelines of the International Council for Harmonisation E6 and the Declaration of Helsinki or local laws and regulations, whichever afforded greater protection. Informed consent was obtained from the patient or their legally authorized representative prior to participation. The studies were approved by institutional review boards or ethics committees at each site.

Reporting summary

Further information on research design is available in the Nature Research Reporting Summary linked to this article.

Data availability

The RNAseq and proteomics data that support the findings of this study are available in the public online respositories Gene Expression Omnibus (GEO), SRA, and the European Genome-Phenome Archive (EGA). COMET: GEO GSE163668 (whole blood), GSE163426 (tracheal aspirate), GSE168453 (PBMC). Schulte-Schrepping, et al.: http://fastgenomics.org. Liao, et al.: SRA PRJNA608742. Silvin, et al.: EGA E-MTAB-9221. Delorey, et al.: Broad Single Cell Portal accession number SCP1052. Grant, et al.: GEO GSE155249. COVACTA RNA-seq, proteomics, and clinical metadata: EGA; accession number EGAS00001006688 (available to qualified researchers upon request; https://ega-archive.org/). Individual patient level clinical data for the COVACTA study is available through the clinical study data request platform (https://vivli.org/).

Code availability

No new algorithms were developed for this manuscript. Most of the analyses performed in this study used published packages mentioned in the Methods, with the exception of the EnhancedVolcano (https://github.com/kevinblighe/EnhancedVolcano) package used to generate volcano plots. All code generated for analysis is available from the authors upon request.

Author Contributions

C.M.R., J.A.H, and H.S. conceived of and designed the overall study. J.A.H., H.S., H.VH., C.O., L.O., X.G., A.C., and C.M.R. performed and interpreted computational analyses. X.G. performed *in vitro* experiments. X.G., N.W., A.Q., D.C., A.C., D.F.C., A.J.C., T.C., G.K.F., A.A.R., A.R., J.T., K.H., N.F.K., M.F.K., D.J.E., K.K., A.S., Z.L., C.S.C., P.G.W., R.G., E.M., A.B., S.Z., C.L., C.M.H., M.G.P.vdW, G.C.H., T.G., R.B., D.S.L., J.R.G., Y.S., R.P., A.O., A.W., C.J.Y., UCSF COMET Consortium, T.R., J.M.M., F.C., A.T., M.B., L.T., I.O.R., A.R., S.B.K., R.N.B., C.M.R. facilitiated the COMET or COVACTA studies and providing data and/or critical feedback on methods and results. C.M.R., J.A.H, and H.S. wrote the first draft of the manuscript. All authors reviewed and approved the final manuscript.

Acknowledgements

UCSF COMET Consortium co-authors: Yumiko Abe-Jones, Michael Adkisson, K. Mark Ansel, Saurabh Asthana, Alexander Beagle, Sharvari Bhide, Cathy Cai, Saharai Caldera, Maria Calvo, Sidney A. Carrillo, Suzanna Chak, Stephanie Christenson, Zachary Collins, Spyros Darmanis, Angela Detweiler, Catherine DeVoe, Walter Eckalbar, Jeremy Giberson, Ana Gonzalez, Gracie Gordon, Paula Hayakawa Serpa, Alejandra Jauregui, Chayse Jones, Serena Ke, Divya Kushnoor, Tasha Lea, Deanna Lee, Aleksandra Leligdowicz, Yale Liu, Salman Mahboob, Lenka Maliskova, Michael Matthay, Elizabeth McCarthy, Priscila Muñoz-Sandoval, Norma Neff, Viet Nguyen, Nishita Nigam, Randy Parada, Maira Phelps, Logan Pierce, Priya Prasad, Sadeed Rashid, Gabriella Reeder, Nicklaus Rodriguez, Bushra Samad, Andrew Schroeder, Cole Shaw, Alan Shen, Austin Sigman, Pratik Sinha, Matthew Spitzer, Sara Sunshine, Kevin Tang, Luz Torres Altamirano, Alexandra Tsitsiklis, Erden Tumurbaatar, Vaibhav Upadhyay, Alexander Whatley, Andrew

Willmore, Michael Wilson, Juliane Winkler, Kristine Wong, Kimberly Yee, Michelle Yu, Mingyue Zhou, Wandi S. Zhu

Funding

This study was supported with funding from Roche, Inc. and federal funds from the Department of Health and Human Services; Office of the Assistant Secretary for Preparedness and Response; Biomedical Advanced Research and Development Authority, under OT number: HHSO100201800036C. C.J.Y. is further supported by the NIH grants R01AR071522, R01AI136972, U01HG012192, and the Chan Zuckerberg Initiative, and is an investigator at the Chan Zuckerberg Biohub and is a member of the Parker Institute for Cancer Immunotherapy (PICI). G.C.H. was supported by the National Science Foundation Undergraduate Research Fellowship Program 1650113. C.S.C. is further supported by NIH R35HL140026. C.H. is further supported by a K23 from NHLBI K23 HL133495.

692 **References**

693 1. Arunachalam, P. S. *et al.* Systems biological assessment of immunity to mild versus
694 severe COVID-19 infection in humans. *Science (1979)* **369**, 1210–1220 (2020).
695 2. Combes, A. J. *et al.* Global absence and targeting of protective immune states in severe
696 COVID-19. *Nature* **591**, 124–130 (2021).
697 3. Zheng, H. *et al.* Multi-cohort analysis of host immune response identifies conserved
698 protective and detrimental modules associated with severity across viruses. *Immunity* **54**,
699 753-768.e5 (2021).
700 4. MacDonald, L. *et al.* COVID-19 and RA share an SPP1 myeloid pathway that drives PD-
701 L1+ neutrophils and CD14+ monocytes. *JCI Insight* **6**, (2021).
702 5. Delorey, T. M. *et al.* COVID-19 tissue atlases reveal SARS-CoV-2 pathology and cellular
703 targets. *Nature* **595**, 107–113 (2021).
704 6. Grant, R. A. *et al.* Circuits between infected macrophages and T cells in SARS-CoV-2
705 pneumonia. *Nature* **590**, 635–641 (2021).
706 7. Liao, M. *et al.* Single-cell landscape of bronchoalveolar immune cells in patients with
707 COVID-19. *Nat Med* **26**, 842–844 (2020).
708 8. Ren, X. *et al.* COVID-19 immune features revealed by a large-scale single-cell
709 transcriptome atlas. *Cell* **184**, 1895-1913.e19 (2021).
710 9. Reyes, M. *et al.* An immune-cell signature of bacterial sepsis. *Nat Med* **26**, 333–340
711 (2020).
712 10. Reyes, M. *et al.* Plasma from patients with bacterial sepsis or severe COVID-19 induces
713 suppressive myeloid cell production from hematopoietic progenitors in vitro. *Sci Transl*
714 *Med* **13**, 9599 (2021).
715 11. Schulte-Schrepping, J. *et al.* Severe COVID-19 Is Marked by a Dysregulated Myeloid
716 Cell Compartment. *Cell* **182**, 1419-1440.e23 (2020).
717 12. Silvin, A. *et al.* Elevated Calprotectin and Abnormal Myeloid Cell Subsets Discriminate
718 Severe from Mild COVID-19. *Cell* **182**, 1401 (2020).
719 13. Rowlands, M., Segal, F. & Hartl, D. Myeloid-Derived Suppressor Cells as a Potential
720 Biomarker and Therapeutic Target in COVID-19. *Front Immunol* **12**, 2435 (2021).
721 14. Shivram, H. *et al.* Tocilizumab treatment leads to early resolution of myeloid dysfunction
722 and lymphopenia in patients hospitalized with COVID-19. *bioRxiv* 2022.10.27.514096
723 (2022) doi:10.1101/2022.10.27.514096.
724 15. LaSalle, T. J. *et al.* Longitudinal characterization of circulating neutrophils uncovers
725 distinct phenotypes associated with severity in hospitalized COVID-19 patients. *Cell Rep*
726 *Med* **3**, 100779 (2022).
727 16. Stephenson, E. *et al.* Single-cell multi-omics analysis of the immune response in COVID-
728 19. *Nat Med* **27**, 904–916 (2021).
729 17. Bost, P. *et al.* Deciphering the state of immune silence in fatal COVID-19 patients. *Nat*
730 *Commun* **12**, 1428 (2021).
731 18. Kvedaraite, E. *et al.* Major alterations in the mononuclear phagocyte landscape associated
732 with COVID-19 severity. *Proc Natl Acad Sci U S A* **118**, (2021).
733 19. Schrijver, I. T., Théroude, C. & Roger, T. Myeloid-Derived Suppressor Cells in Sepsis.
734 *Front Immunol* **10**, 327 (2019).
735 20. Gabrilovich, D. I. & Nagaraj, S. Myeloid-derived suppressor cells as regulators of the
736 immune system. *Nature Reviews Immunology 2009 9:3* **9**, 162–174 (2009).

21. Veglia, F., Sanseviero, E. & Gabrilovich, D. I. Myeloid-derived suppressor cells in the era of increasing myeloid cell diversity. *Nat Rev Immunol* **21**, 485–498 (2021).
22. Hegde, S., Leader, A. M. & Merad, M. MDSC: Markers, development, states, and unaddressed complexity. *Immunity* **54**, 875–884 (2021).
23. Agrati, C. *et al.* Expansion of myeloid-derived suppressor cells in patients with severe coronavirus disease (COVID-19). *Cell Death Differ* **27**, 3196–3207 (2020).
24. Darcy, C. J. *et al.* Neutrophils with myeloid derived suppressor function deplete arginine and constrain T cell function in septic shock patients. *Crit Care* **18**, R163 (2014).
25. Dean, M. J. *et al.* Severe COVID-19 Is Characterized by an Impaired Type I Interferon Response and Elevated Levels of Arginase Producing Granulocytic Myeloid Derived Suppressor Cells. *Front Immunol* **12**, 695972 (2021).
26. Falck-Jones, S. *et al.* Functional monocytic myeloid-derived suppressor cells increase in blood but not airways and predict COVID-19 severity. *Journal of Clinical Investigation* **131**, (2021).
27. Reizine, F. *et al.* SARS-CoV-2-Induced ARDS Associates with MDSC Expansion, Lymphocyte Dysfunction, and Arginine Shortage. *J Clin Immunol* **41**, 515–525 (2021).
28. Sacchi, A. *et al.* Early expansion of myeloid-derived suppressor cells inhibits SARS-CoV-2 specific T-cell response and may predict fatal COVID-19 outcome. *Cell Death Dis* **11**, 921 (2020).
29. Tom, J. *et al.* Prognostic and Predictive Biomarkers in Patients with Coronavirus Disease 2019 Treated with Tocilizumab in a Randomized Controlled Trial∗. *Crit Care Med* **50**, 398–409 (2022).
30. Bunt, S. K. *et al.* Reduced Inflammation in the Tumor Microenvironment Delays the Accumulation of Myeloid-Derived Suppressor Cells and Limits Tumor Progression. *Cancer Res* **67**, 10019 (2007).
31. Chen, G. *et al.* Clinical and immunological features of severe and moderate coronavirus disease 2019. *J Clin Invest* **130**, 2620–2629 (2020).
32. Oh, K. *et al.* A mutual activation loop between breast cancer cells and myeloid-derived suppressor cells facilitates spontaneous metastasis through IL-6 trans-signaling in a murine model. *Breast Cancer Research* **15**, R79 (2013).
33. Weber, R. *et al.* IL-6 as a major regulator of MDSC activity and possible target for cancer immunotherapy. *Cell Immunol* **359**, 104254 (2021).
34. Rosas, I. O. *et al.* Tocilizumab in Hospitalized Patients with Severe Covid-19 Pneumonia. *N Engl J Med* **384**, 1503–1516 (2021).
35. Shankar-Hari, M. *et al.* Association Between Administration of IL-6 Antagonists and Mortality Among Patients Hospitalized for COVID-19: A Meta-analysis. *JAMA* **326**, 499–518 (2021).
36. Sarma, A. *et al.* Tracheal aspirate RNA sequencing identifies distinct immunological features of COVID-19 ARDS. *Nature Communications 2021 12:1* **12**, 1–10 (2021).
37. van der Wijst, M. G. P. *et al.* Type I interferon autoantibodies are associated with systemic immune alterations in patients with COVID-19. *Sci Transl Med* **13**, eabh2624 (2021).
38. Su, Y. *et al.* Multi-Omics Resolves a Sharp Disease-State Shift between Mild and Moderate COVID-19. *Cell* **183**, 1479 (2020).
39. Aschenbrenner, A. C. *et al.* Disease severity-specific neutrophil signatures in blood transcriptomes stratify COVID-19 patients. *Genome Medicine 2021 13:1* **13**, 1–25 (2021).

40. Hasegawa, T. *et al.* The regulation of EN-RAGE (S100A12) gene expression in human THP-1 macrophages. *Atherosclerosis* **171**, 211–218 (2003).
41. Lorenz, E. *et al.* Different expression ratio of S100A8/A9 and S100A12 in acute and chronic lung diseases. *Respir Med* **102**, 567–573 (2008).
42. Medina, E. & Hartl, D. Myeloid-Derived Suppressor Cells in Infection: A General Overview. *J Innate Immun* **10**, 407–413 (2018).
43. Eisemann, T., Costa, B., Peterziel, H. & Angel, P. Podoplanin Positive Myeloid Cells Promote Glioma Development by Immune Suppression. *Front Oncol* **9**, 187 (2019).
44. Karakasheva, T. A. *et al.* CD38-expressing myeloid-derived suppressor cells promote tumor growth in a murine model of esophageal cancer. *Cancer Res* **75**, 4074–4085 (2015).
45. Newman, A. M. *et al.* Robust enumeration of cell subsets from tissue expression profiles. *Nature Methods 2015 12:5* **12**, 453–457 (2015).
46. Zhou, R. *et al.* Acute SARS-CoV-2 Infection Impairs Dendritic Cell and T Cell Responses. *Immunity* **53**, 864 (2020).
47. Meckiff, B. J. *et al.* Imbalance of Regulatory and Cytotoxic SARS-CoV-2-Reactive CD4+ T Cells in COVID-19. *Cell* **183**, 1340 (2020).
48. Files, J. K. *et al.* Sustained cellular immune dysregulation in individuals recovering from SARS-CoV-2 infection. *J Clin Invest* **131**, (2021).
49. Wilk, A. J. *et al.* A single-cell atlas of the peripheral immune response in patients with severe COVID-19. *Nat Med* **26**, 1070–1076 (2020).
50. Diao, B. *et al.* Reduction and Functional Exhaustion of T Cells in Patients With Coronavirus Disease 2019 (COVID-19). *Front Immunol* **11**, 827 (2020).
51. Mathew, D. *et al.* Deep immune profiling of COVID-19 patients reveals distinct immunotypes with therapeutic implications. *Science (1979)* **369**, (2020).
52. Zheng, M. *et al.* Functional exhaustion of antiviral lymphocytes in COVID-19 patients. *Cell Mol Immunol* **17**, 533–535 (2020).
53. Galván-Peña, S. *et al.* Profound Treg perturbations correlate with COVID-19 severity. *Proceedings of the National Academy of Sciences* **118**, e2111315118 (2021).
54. Fahey, E. & Doyle, S. L. IL-1 Family Cytokine Regulation of Vascular Permeability and Angiogenesis. *Front Immunol* **10**, 1426 (2019).
55. Pittet, J.-F. *et al.* TGF-β is a critical mediator of acute lung injury. *Journal of Clinical Investigation* **107**, 1537 (2001).
56. R Core Team. R: A language and environment for statistical computing. *R Foundation for Statistical Computing, Vienna, Austria.* (2020).
57. McCarthy, D., Campbell, K., Lun, A. & Wills, Q. scater: pre-processing, quality control, normalisation and visualisation of single-cell RNA-seq data in R. *Scater: Pre-processing, quality control, normalization and visualization of single-cell RNA-seq data in R* 069633 (2016) doi:10.1101/069633.
58. Lun, A. T. L., McCarthy, D. J. & Marioni, J. C. A step-by-step workflow for low-level analysis of single-cell RNA-seq data with Bioconductor. *F1000Res* **5**, (2016).
59. Lun, A. T. L. *et al.* EmptyDrops: Distinguishing cells from empty droplets in droplet-based single-cell RNA sequencing data. *Genome Biol* **20**, 1–9 (2019).
60. Robinson, M. D., McCarthy, D. J. & Smyth, G. K. edgeR: a Bioconductor package for differential expression analysis of digital gene expression data. *Bioinformatics* **26**, 139–140 (2010).

61. Bueno, R. *et al.* Comprehensive genomic analysis of malignant pleural mesothelioma identifies recurrent mutations, gene fusions and splicing alterations. *Nature Genetics 2016 48:4* **48**, 407–416 (2016).
62. Hao, Y. *et al.* Integrated analysis of multimodal single-cell data. *Cell* **184**, 3573-3587.e29 (2021).
63. Wolf, F. A., Angerer, P. & Theis, F. J. SCANPY: large-scale single-cell gene expression data analysis. *Genome Biol* **19**, 15 (2018).
64. Pau G, R. J. HTSeqGenie: A NGS analysis pipeline. *R package version 4.22.0.* (2013).
65. Bernard, G. R. *et al.* The American-European Consensus Conference on ARDS. Definitions, mechanisms, relevant outcomes, and clinical trial coordination. *Am J Respir Crit Care Med* **149**, 818–824 (1994).
66. Ranieri, V. M. *et al.* Acute respiratory distress syndrome: The Berlin definition. *JAMA - Journal of the American Medical Association* **307**, 2526–2533 (2012).
67. Angelova, M. *et al.* Characterization of the immunophenotypes and antigenomes of colorectal cancers reveals distinct tumor escape mechanisms and novel targets for immunotherapy. *Genome Biology 2015 16:1* **16**, 1–17 (2015).

845 **Tables**
846
847 **Table 1. Patient characteristics**
848 NA = not available. COVACTA data are for subjects with blood RNA-seq data included in this
849 manuscript. COVACTA ICU admission frequency is at time of baseline sampling.
850

	COMET			COVACTA
	All	SARS-CoV-2+	SARS-CoV-2-	
n (%)	75	57 (76%)	18 (24%)	404
Age median (IQR)	54 (42, 69)	48 (42, 66)	66 (51, 76)	63 (53-70)
Sex				
Male n (%)	52 (69%)	43 (75%)	9 (50%)	284 (70%)
Female n (%)	23 (31)	14 (25%)	9 (50%)	120 (30%)
Race n (%)				
White	20 (27%)	11 (19%)	9 (50%)	233 (58%)
Black/African American	4 (5%)	3 (5%)	1 (6%)	58 (14%)
Asian	13 (17%)	9 (16%)	4 (22%)	37 (9%)
Other/Mixed/Unknown	38 (51%)	34 (60%)	4 (22%)	76 (19%)
Baseline NIH Ordinal Scale n (%)				
3 No supplemental O2	14 (19%)	12 (21%)	2 (11%)	15 (4%)
4 Supplemental O2	25 (33%)	18 (32%)	7 (39%)	109 (27%)
5 Non-invasive/high flow O2	14 (19%)	9 (16%)	5 (28%)	114 (28%)
6 Mechanical ventilation (MV)	3 (4%)	3 (5%)	0 (0%)	58 (14%)
7 MV + additional organ support	19 (25%)	15 (26%)	4 (22%)	107 (27%)
SOFA maximal median (IQR)	4 (1, 10)	4 (1, 11)	4 (1, 9)	NA
ICU admission n (%)	26 (35%)	30 (53%)	11 (61%)	234 (58%)
Mortality n (%)	10 (13%)	6 (11%)	4 (22%)	83 (20%)
ARDS AECC definition n (%)	38 (51%)	26 (46%)	12 (67%)	NA
ARDS Berlin definition n (%)	23 (31%)	18 (32%)	5 (28%)	NA
Hospitalization, days median (IQR)	8 (8, 18)	11 (3, 20)	5 (4, 7)	22 (9-28)
ICU duration, days median (IQR)	2 (0, 9)	14 (4, 26)	4 (2, 4)	14 (0-27)
Ventilator-free days median (IQR)	28 (18, 28)	28 (16, 28)	28 (26, 28)	19 (0-28)

851
852
853

Figures

Figure 1. Identification of the severity-associated EN-RAGE myeloid signature in COVID-19 airway (BAL) and peripheral (PBMC) samples.
A. Pairwise Pearson correlation between all genes and S100A12 in either PBMC[11] or BAL[7].
B. Pseudo-bulk expression profiles of PBMC and BAL. Each point represents a patient. Blue=healthy (BAL n = 3; PBMC, n = 3), yellow=moderate/severe (BAL, n = 3; PBMC, n = 8; hospitalized -/+ supplemental O_2), red=critical (BAL, n = 6; PBMC, n = 10; requiring mechanical ventilation), with severity defined within each dataset by the authors. Increased expression in severe patients in both tissues. Significance was tested using a t-test across the indicated groups (n.s. = $p > 0.05$, * = $p < 0.05$; ** = $p < 0.01$; *** = $p < 0.001$).

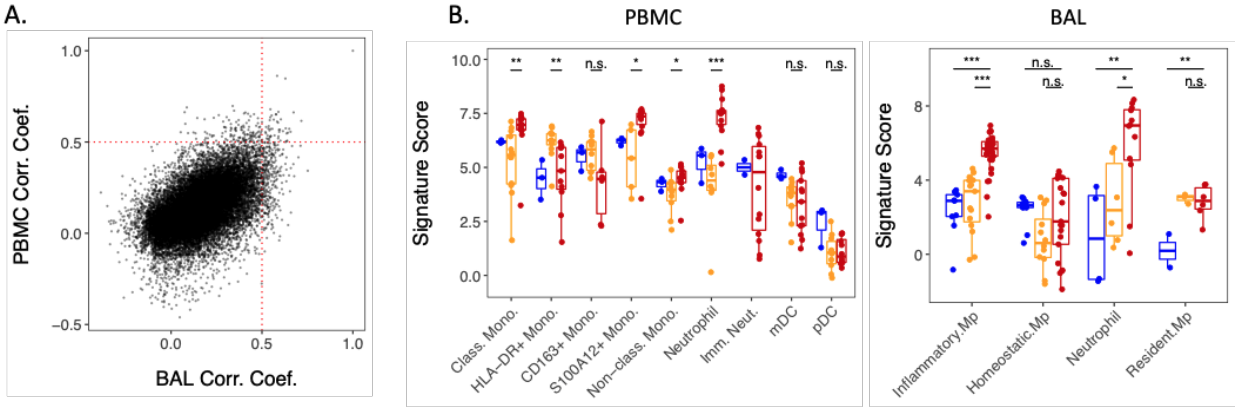

Figure 2. Replication of EN-RAGE severity association across sample types in both COVID-19 and non-COVID-19 acute lung injury (COMET cohort).

A. UMAP plots with cell type annotations. Each point represents a single cell, colored by cell type. Each panel shows a different sample type, as indicated. PBMC: peripheral blood mononuclear cells, WB: whole blood, ETA:endotracheal aspirates.

B. UMAP plots showing EN-RAGE signature score. Each point represented a single cell colored by the expression signature value.

C. Pseudo-bulk expression profiles within myeloid cells. Each point represents the pseudo-bulk gene expression signature score for a cell type in a patient sample. PBMC severity: Moderate = no supplemental O_2, severe = supplemental O_2 and critical = mechanical ventilation. Whole blood severity: Mild/Moderate = 0 days on ventilator and no more than 1 day in ICU, Severe patients had ≥1 day on ventilator. ETA: Critical=VFDS=0 (ventilation for ≥28 days or death), severe ETA=VFDS>0. Significance was tested using a t-test across the indicated groups (n.s. = $p > 0.05$, ** = $p < 0.01$; *** = $p < 0.001$). Sample numbers per cohort: PBMC healthy, n = 11; PBMC COVID- moderate, n = 4; PBMC COVID- severe, n = 6; PBMC COVID- critical, n = 3; PBMC COVID+ moderate, n = 12; PBMC COVID+ severe, n = 10; PBMC COVID+ critical, n = 14. WB healthy, n = 14; WB COVID- mild, n = 4; WB COVID- severe, n = 1; WB COVID+ mild, n = 8; WB COVID+ severe, n = 5. ETA COVID- moderate/severe, n = 2; ETA COVID- critical, n = 1; ETA COVID+ moderate/severe, n = 5; ETA COVID+ critical, n = 8.

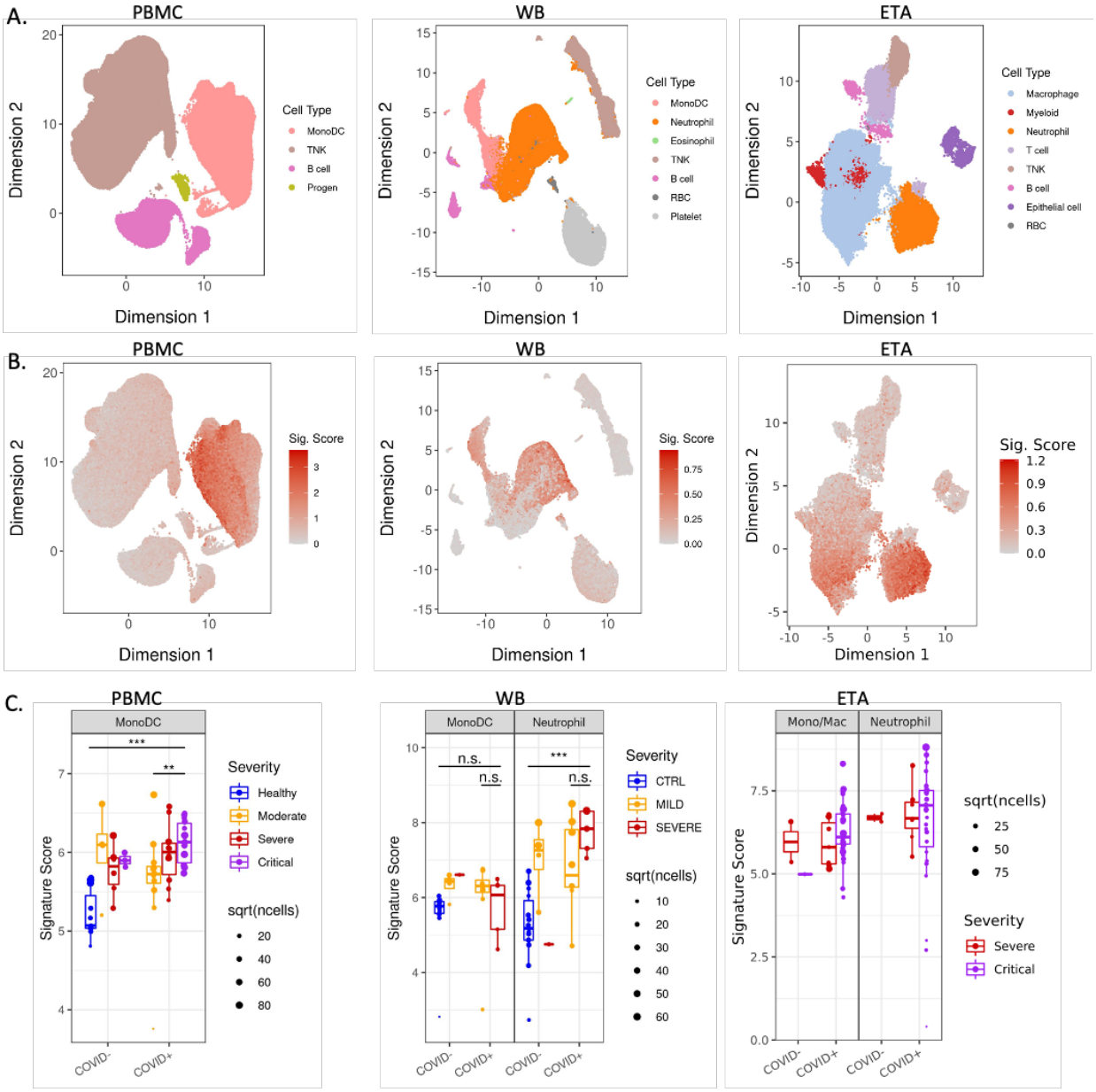
A.
PBMC
WB
ETA
Dimension 1
Dimension 2
Cell Type
MonoDC
TNK
B cell
Progen
Neutrophil
Eosinophil
RBC
Platelet
Macrophage
Myeloid
T cell
Epithelial cell
B.
Sig. Score
C.
MonoDC
Neutrophil
Mono/Mac
Signature Score
Severity
Healthy
Moderate
Severe
Critical
CTRL
MILD
SEVERE
sqrt(ncells)
COVID-
COVID+
n.s.
***
**

890 **Figure 3.** EN-RAGE signature expression correlates with disease severity and immunosuppressive
891 gene expression in myeloid cells (COMET cohort).
892 **A.** Spearman correlations between pseudo-bulk EN-RAGE signature score in PBMC monocytes
893 and NIH ordinal severity score, maximal NIH severity score, SOFA organ failure score, and
894 plasma IL-6 and IL-10 protein levels at study enrollment. **B.** PBMC monocyte EN-RAGE gene
895 score is higher in patients who develop ARDS (AECC definition) in COVID-19 patients; n=46.
896 Medians are indicated. * t-test $p<0.05$. **C.** Longitudinal changes in EN-RAGE signature in bulk
897 ETA RNA-seq. Each point represents a patient sample from COVID-19 (n=16 patients, n=276
898 samples) and non-COVID (n=3 patients, n=6 samples) patients requiring mechanical ventilation.
899 Samples from the same patient are linked by dotted lines. Points are colored by severity of disease.
900 For illustrative purposes, linear regression trend lines for signature scores over time, grouped by
901 severity level are shown as solid lines. Slopes were significantly different using a linear mixed
902 model, $p<0.05$. MV=mechanical ventilation. **D.** Table of Spearman correlation coefficients
903 between pseudo-bulk EN-RAGE signature score and genes encoding myeloid effector functions
904 within monocyte or neutrophil populations across endotracheal aspirates (ETA), whole blood, and
905 PBMCs from the COMET cohort. Positive correlations are shaded red and negative correlations
906 shaded blue, with increasing darkness of shading indicating two tailed p values of $p<0.05$, $p<0.01$,
907 and $p<0.001$. **E.** PBMC myeloid EN-RAGE gene score correlates with plasma IL-6 and IL-10
908 protein; n=46. **F.** Correlation of pseudo-bulk expression signature for EN-RAGE genes compared
909 to pseudo-bulk expression values of IL-10 and PD-L1 in monocytes in COMET tracheal aspirate
910 samples. Each point represents the expression value in a cell type in a single sample; n=40. Log_2
911 gene expression, Spearman correlation coefficients and two tailed p values are shown.
912

A

		Clinical severity		Clinical outcome		Plasma protein	
PBMC		NIH	SOFA	NIH MAX	VFDS	IL-6	IL-10
Monocyte	r	0.37	0.22	0.30	-0.25	0.41	0.29
	p	0.010	0.15	0.02	0.10	0.005	0.05

B

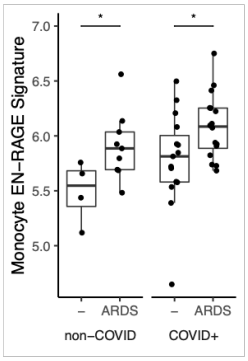

C

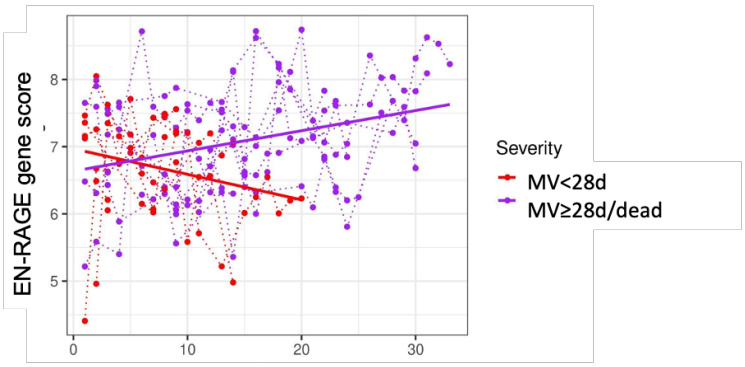

D

		Lung recruitment/phenotype						T cell suppression					
Spearman rho		HLA.DRA	HLA.DRB1	CD14	CCR2	PTGER2	STAT3	ENRAGE	IL10	PDL1	IL1B	CYBB	TGFB1
ETA	n												
Monocyte	41	0.11	-0.23	0.09	0.26	0.72	0.75	0.70	0.74	0.59	0.86	0.14	0.13
Neutrophil	40	0.03	-0.16	0.58	0.00	0.35	0.63	0.74	0.53	0.59	0.78	0.21	0.54
Blood	n												
Monocyte	18	-0.01	0.19	0.62	0.53	0.52	0.79	0.67	0.57	0.31	0.34	0.60	0.37
Neutrophil	18	-0.53	-0.52	0.78	-0.21	-0.48	0.94	0.72	0.27	0.78	0.70	0.28	0.91
PBMC	n												
Monocyte	44	-0.45	-0.48	0.65	0.25	0.38	0.15	0.73	0.15	0.02	0.34	0.52	0.18

E PBMC

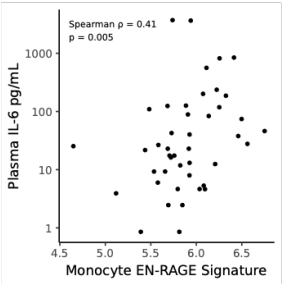

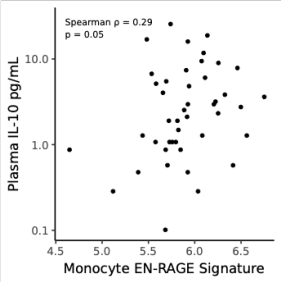

F ETA

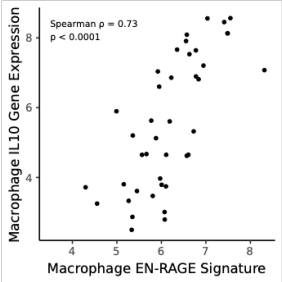

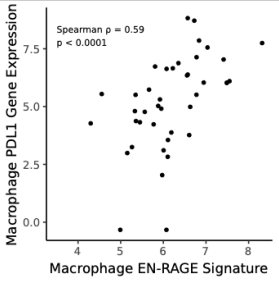

Figure 4. Characterization of myeloid and T cell immunosuppression phenotypes (COMET PBMC cohort).

A. EN-RAGE gene set score is most highly expressed in classical monocytes (cM) in PBMC CITE-seq data. ncM=non-classical monocytes, progen=progenitor cells. B. CD14, CD16, and HLA-DR surface protein expression across cell lineages in PBMC CITE-seq data. C-E. Spearman correlations between EN-RAGE gene set expression in classical monocytes and protein expression on C. classical monocytes, D. $CD4^+$ T cells and E. $CD8^+$ cells; n=128 samples, including 11 healthy controls. FDR<0.05 for all correlations, panel of 188 proteins measured. F-L Pseudobulked surface protein expression in 128 PBMC samples from 60 patients over 14 days in patients grouped by clinical outcomes. Classical monocyte expression of F. EN-RAGE gene signature, G. HLA-DR protein, H. PD-L1 protein. $CD8^+$ T cell expression of I. PD-1 and J. LAG3. $CD4^+$ T cell expression of K. PD-1 and L. LAG3. Blue line denotes the linear regression trend for gene expression over time. Red line denotes expression level in healthy controls. Vent. duration = days of mechanical ventilation in survivors. n=128 samples from 60 patients (429, 505 cells). Pearson correlation coefficients (r) and p values are indicated.

934

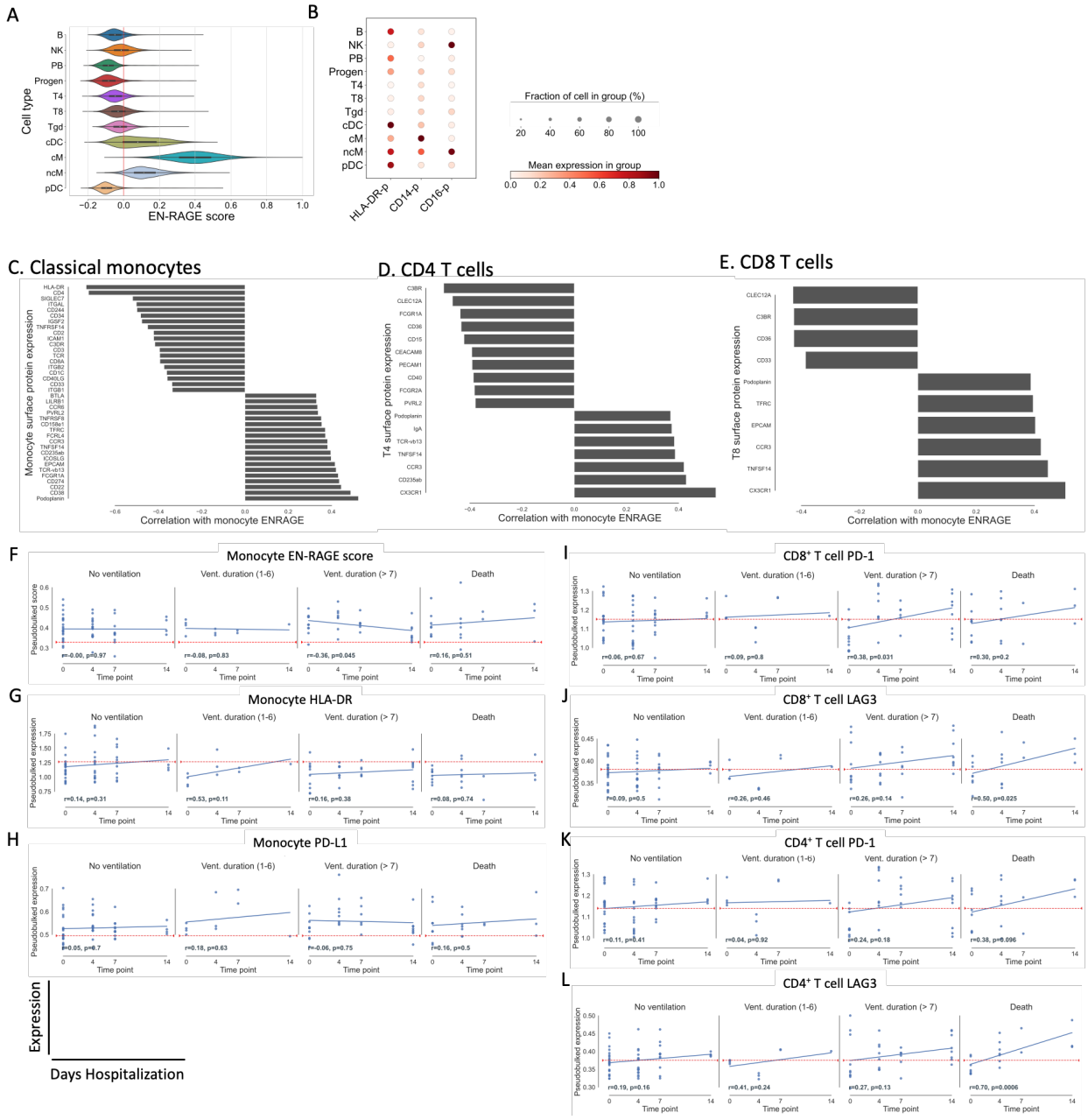
A
Cell type
B
NK
PB
Progen
T4
T8
Tgd
cDC
cM
ncM
pDC
EN-RAGE score
B
HLA-DR-p
CD14-p
CD16-p
Fraction of cell in group (%)
Mean expression in group
C. Classical monocytes
Monocyte surface protein expression
Correlation with monocyte ENRAGE
D. CD4 T cells
T4 surface protein expression
Correlation with monocyte ENRAGE
E. CD8 T cells
T8 surface protein expression
Correlation with monocyte ENRAGE
F
Monocyte EN-RAGE score
G
Monocyte HLA-DR
H
Monocyte PD-L1
I
CD8+ T cell PD-1
J
CD8+ T cell LAG3
K
CD4+ T cell PD-1
L
CD4+ T cell LAG3
No ventilation
Vent. duration (1-6)
Vent. duration (> 7)
Death
Pseudobulked score
Pseudobulked expression
Time point
Expression
Days Hospitalization

935

936

Figure 5. IL-6 treatment of monocytes in vitro induces a gene program associated with severity and potential T cell suppression

A. Differentially expressed EN-RAGE genes in human monocytes stimulated with IL-6 for 24 hours compared with media. Heat map of the genes with FDR<0.05 using unsupervised clustering, along with IL-10. B. FGSEA analysis of EN-RAGE and MS1 signatures in IL-6 treated monocytes. Bars represent the normalized enrichment scores of how much each gene set is regulated by IL-6 treatment (BH adjusted p-value for MS1 < 0.01 and EN-RAGE < 0.001).

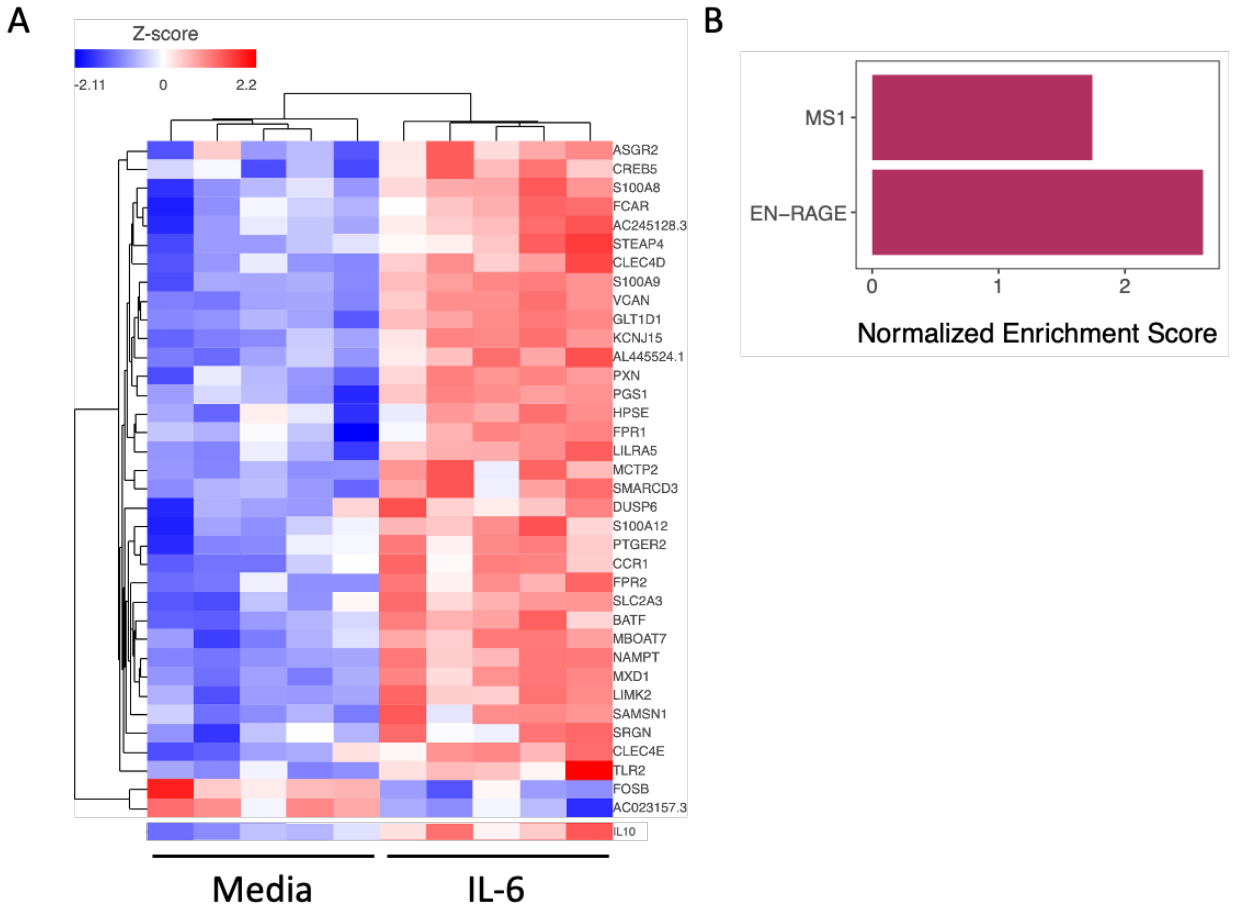

Figure 6. Severity-associated EN-RAGE gene set is associated with poor outcome and decreased by IL-6 blockade in COVID-19 patients (COVACTA cohort). **A.** Heatmap of EN-RAGE gene set associations with NIH ordinal scale severity at D1 (Severity NIH), need for new mechanical ventilation in patients not ventilated on D1 (Mech Vent), 28 day mortality (Death), treatment with tocilizumab or placebo at D3 or D7 relative to D1, and tocilizumab (TCZ) vs placebo at D7 relative to D1. **B-E.** Gene set enrichment analyses (GSEA) for gene sets associated with the myeloid cell states EN-RAGE, MS1[10], and MDSC[67] and T cells (CIBERSORT[45]). Normalized enrichment scores are shown, with red shading for t test $p<0.05$ and grey for $p>0.05$. TCZ = tocilizumab. For C and D, analyses were adjusted for baseline severity by incorporating baseline ordinal score as a covariate in our model. **F-G.** Tocilizumab treatment normalizes (F) EN-RAGE and (G) $CD8^+$ T cell gene expression to healthy levels more rapidly than placebo in survivors. Only patients with measurements for all three time points are included. Lines represent the mean expression value for the gene set signature score across tocilizumab- or placebo-treated subjects. Error bars represent the 95% confidence interval around the mean. Patients are split into those that were discharged before 28, those that remained hospitalized, or subjects that died by day 28. Average signature scores are shown across the first 7 days of treatment. CTRL=healthy controls, SOC = standard of care drug therapy; significance testing was performed using t-test comparing each day to D1 by study arm * = $p < 0.05$, ** = $p < 0.01$, *** = $p < 0.001$, **** = $p < 0.0001$.

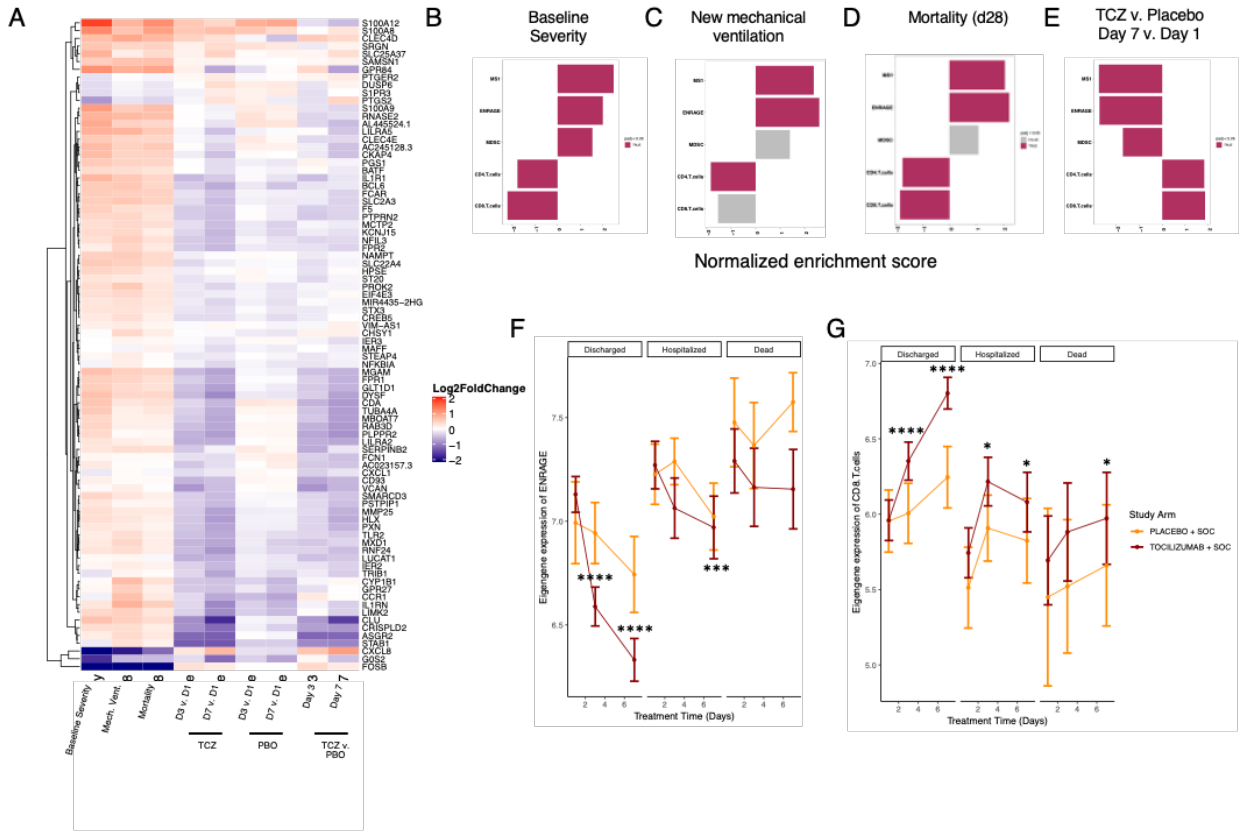
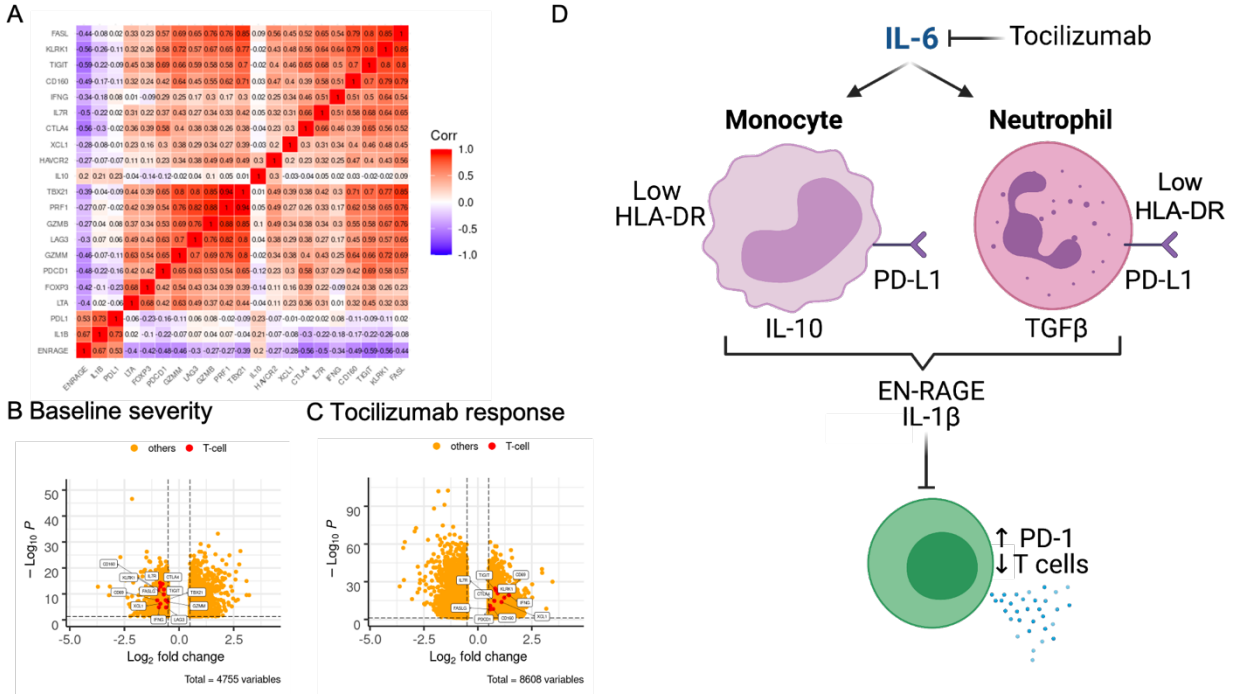
Figure 7. IL-6 blockade reduces potential T cell suppressive factors and normalizes T cells in COVID-19 patients (COVACTA cohort). A. EN-RAGE is positively correlated with IL-6-induced suppressive myeloid genes (*IL-10, IL-1b, PD-L1*) and inversely correlated with T cell genes (*FASL, LKRK1, TIGIT, CD160, IFNG, IL7R, CTLA4, XCL1, HAVCR2, TBX21, PRF1, GZMB, LAG3, GZMM, PDCD1, FOXP3*). Spearman correlation coefficients are shown for bulk whole blood gene expression. B-C. Volcano plots of reduced expression of T cell genes in A in patients with greater baseline severity (requiring positive pressure ventilation) versus not (B) and increased expression of T cell genes following 7 days treatment with tocilizumab (C). Dotted lines indicate absolute > 0.5 $\log_2$ fold change and FDR<0.05. D. Working model.